Optimal Energy Flow in Integrated Electricity and Gas Systems With Injection of Alternative Gas

Sheng Wang, *Member, IEEE,* Junyi Zhai, *Member, IEEE,* Hongxun Hui, *Member, IEEE*

***Abstract*—This paper proposes an optimal energy flow technique for the integrated electricity and gas systems (IEGS) with injections of alternative gases. Firstly, we develop a novel optimal energy flow model of IEGS with alternative gases, where the physical characteristics (e.g., specific gravity) of the gas mixtures are modeled as variables to reflect the impacts of alternative gas injections more accurately. Security indices are introduced to restrain the gas composition variation. Then, convex optimization techniques are tailored to transfer the original highly nonlinear and nonconvex optimization problem into a tractable form. An advanced sequential programming procedure is proposed with self-adaptive convergence criteria to better balance the feasibility and convergency. Finally, the IEEE 24-bus RTS and Belgium gas transmission system, and the practical 160-bus Britain gas system are used to validate the proposed techniques. It can be observed from numerical studies that the computation efficiency of the proposed solution methods is 96.44% faster than traditional mixed-integer nonlinear solvers. The injection of alternative gas can cause up to 4.32% variations in the nodal gas pressure. Nonetheless, under various uncertainties from renewable generation, load level, etc., the proposed optimal energy flow model can maintain the security of IEGS.**

***Index Terms*—optimal energy flow, integrated electricity and gas systems, alternative gas, gas system security, convex optimization.**

NOMENCLATURE

A. Acronyms

GCV	Gross caloric value
GPP	Gas-fired power plants
IEGS	Integrated electricity and gas systems
LPG	Liquefied petroleum gas
MISOC	Mixed-integer second order cone
OEF	Optimal energy flow
PTG	Power to gas
RTS	Reliability test system
TPP	Traditional fossil power plant

B. Indices

i, j	Index for bus
l	Index for system components (gas source, TPPs, etc.)
r	Index for gas component
v	Index for iteration

C. Sets, matrixes, and functions

$\boldsymbol{\xi}^{\mathrm{SI}}$	Set of thresholds for security indices
$\boldsymbol{SI}_i$	Set of security indices at bus i
$\mathcal{GP}$	Set of gas pipelines
$\mathcal{I}$	Set of buses
$\mathcal{J}_i$	Set of buses connected to bus i
$\mathcal{L}_i^{\mathrm{gpp}}$	Set of GPPs at bus i
$\mathcal{L}_i^{\mathrm{gpp}}$	Set of TPPs at bus i
$\mathcal{L}_i^{\mathrm{ptg}}$	Set of PTGs at bus i
$\mathcal{L}_i^{\mathrm{rng}}$	Set of renewable generators at bus i
$\mathcal{L}_i^{\mathrm{s}}$	Set of gas sources at bus i
$cst_{i,l}$	Generating cost of TPP l at bus i
$f^{(v)}$	Objective function at iteration v
f_{Z}	Function of compressibility factor
$\boldsymbol{q}_{i,l}^{\mathrm{s}}$	Gas supply vector of gas source l at bus i
$\mathcal{R}$	Set of gas components

D. Variables

$\gamma_{i,j}$	Gas flow direction of pipeline ij
$\omega_{i,j}$	Auxiliary variable in the McCormick envelope
$\Phi_{i,j}$	Auxiliary variable for pipeline ij
$\sigma_{i,j}^{\Phi,(v)}$	Slack variable for $\Phi_{i,j}$ at v_{th} iteration
$\sigma_{i,j}^{x,(v)}$	Upper bound of $\varepsilon_{i,r}^{x,(v)}$
$\varepsilon_{i,r}^{x,(v)}$	Slack variable for the Taylor remainders
C^{T}	Total operating cost
CP_i	Combustion potential at bus i
FS_i	Weaver flame speed factor at bus i
GCV_i	GCV of the gas mixture at bus i
$I_{i,j}$	Square of current magnitude of branch i, j
p_i	Gas pressure at bus i
p_i^{s}	Square of gas pressure at bus i
$P_{i,j}$	Active power of electricity flow from bus i to j
$P_{i,l}^{\mathrm{gpp}}$	Active power of GPP l at bus i
$P_{i,l}^{\mathrm{ptg}}$	Electricity consumed by PTG l at bus i
$q_{i,j,r}$	Gas flow of gas composition r in pipeline ij
$Q_{i,j}$	Reactive power of electricity flow from bus i to j
$q_{i,j}$	Total gas flow from bus i to bus j
$q_{i,l,r}^{\mathrm{gpp}}$	Consumption of gas composition r of GPP l at bus i
$q_{i,l,r}^{\mathrm{ptg}}$	Production of gas composition r of PTG l at bus i
$q_{i,l,r}^{\mathrm{s}}$	Supply of gas component r of gas source l at bus i
$Q_{i,l}^{\mathrm{gpp}}$	Reactive power of GPP l at bus i
$q_{i,l}^{\mathrm{hy}}$	Hydrogen production of PTG l at bus i
$q_{i,l}^{\mathrm{me}}$	Methane production of PTG l at bus i
$q_{i,r}^{\mathrm{d}}$	Demand of gas component r at bus i
$S_{i,j}$	Specific gravity of gas mixture in pipeline ij
V_i	Square of magnitude of voltage at bus i
$W_{i,r}$	Nodal injection of gas composition r at bus i
W_i	Total nodal injection of gas at bus i
WI_i	Wobbe index of the gas mixture at bus i
$x_{i,r}$	Molar fraction of gas component r at bus i
$x'_{i,r}, S'_i$	Corrections of gas composition and specific gravity
$Z_{i,j}$	Compressibility factor of gas mixture in pipeline ij

E. Parameters

α	Upper bounds of penalty factors
$\boldsymbol{q}_{i,l}^{\mathrm{s,max}}$	Upper bound of gas supply for gas source l at bus i
$\boldsymbol{q}_{i,l}^{\mathrm{s,min}}$	Lower bound of gas supply for gas source l at bus i
ϵ	Residual tolerance
$\eta_{i,l}^{\mathrm{e}}, \eta_{i,l}^{\mathrm{me}}$	Efficiencies of electrolysis and methanation processes
$\eta_{i,l}^{\mathrm{gpp}}$	Efficiency of GPP l
κ	Multiplier of penalty factor
λ	Penalty factor
μ	Subsidy price for the green gas production
$\phi_{i,l}$	Power factor of renewable generator l at bus i
$\rho_{i,l}^{\mathrm{s}}$	Nodal price for the gas production of gas source l at

	bus i
a_r	Combustion potential coefficient for gas component r
AF	Air-fuel ratio
$C_{i,j}$	Property parameter of pipeline ij
$D_{i,j}$	Diameter of pipeline ij
d_i^{ng}	Original gas demand at bus i
$F_{i,j}$	Friction factor of pipeline ij
fs_r	Burning velocity of gas component r
GCV^{hy}	GCV of hydrogen
GCV^{me}	GCV of methane
GCV^{ng}	GCV of natural gas
GCV_r	GCV of gas component r
$L_{i,j}$	Length of pipeline ij
M^{air}	Molecular weights of air
M_r	Molecular weights of gas component r
O_X	Oxygen index
p^{stp}	Pressure at standard condition
$P_i^{\text{d}}, Q_i^{\text{d}}$	Active and reactive electricity demands at bus i
R^{air}	Gas constant of air
$R_{i,j}$	Resistance of branch ij
S^{ng}	Specific gravity of natural gas
$SL_{i,j}^{\max}$	Apparent capacity of branch ij
T^{stp}	Temperature at standard condition
$x_i^{\text{N}}, x_i^{\text{O}}$	Molar fractions of inert gas and oxygen at bus i
$X_{i,j}$	Reactance of branch ij
$x_{i,l,r}^{\text{s}}$	Molar fraction of gas component r of gas source l at bus i

I. Introduction

THE adoption of gas-fired power plants (GPP) and power-to-gas (PTG) facilities has intensified the interaction between the electricity and gas systems in a bidirectional way. The PTG facilities usually consume surplus renewable generations to produce green hydrogen and methane, which can be injected into the natural gas transmission pipelines for further use [1]. Together with biogas, they are commonly viewed as alternative renewable gases for the decarbonization of integrated electricity and gas systems (IEGS). In recent years, many demonstration projects on hydrogen blending are under construction worldwide. For example, in Chaoyang, China, in 2019, the first demonstration project on green hydrogen blending into natural gas is committed, where the gas network operates with 10% hydrogen for one year [2]. The UK launched its first project HyDeploy in 2019. The first phase is implemented in Keele University's private gas network, which supports the gas demands from 100 homes and 30 university buildings [3].

However, the injection of alternative gases into the existing natural gas transmission system may lead to potential risks. 1) Hydrogen has a lower ignition point and higher burning rate compared with natural gas, which is more likely to cause fire hazards [4]. 2) Gas appliances are usually designed and tested at a given pressure with a specific type of gas. They may not perform satisfactorily if the gas composition changes [5]. 3) The components in the gas network, such as the pipeline, compressor, valve, etc., are also designed for the pre-specified gas composition. Technical issues like hydrogen embrittlement can emerge with a different gas composition [6]. 4) The variation of the gas composition can change the physical characteristics (e.g., specific gravity) of the gas mixtures, which may further lead to the variation of nodal gas pressures and linepack swing patterns, etc. [7]. Nonetheless, compared with the benefits, these security issues can be well contained if the gas composition can be strictly controlled [8].

The literature review on the operation of IEGS with alternative gas injections is summarized in Table. I. Most of the previous studies focus on the simulation of the impacts of alternative gas injections on the gas system or IEGS. The impacts of hydrogen injections on the thermal dynamics and transportation properties of natural gas are investigated in [9]. The dynamic behavior of non-isothermal compressible natural gases with hydrogen in pipelines is modeled in [10]. The composition tracking of natural gas and hydrogen mixtures in the gas network under dynamic conditions is studied in [11]. The simulation technique of the gas composition in the gas network is proposed in [12]. Dynamics of natural gas quality with hydrogen injections in a single transmission pipeline are modeled in [13]. The gas composition tracking is further extended to the transient conditions in [14], and special treatment is done to avoid convection-dominated oscillations in numerical methods. The dynamic modeling and characteristic analysis of natural gas systems with hydrogen injection are analyzed in [15].

Some studies extend the simulations to the IEGS. The IEGS with hydrogen blending is modeled to address the increasingly distributed photovoltaic generation in [16]. The gas distribution network is also used to absorb the excess renewable electricity generations through hydrogen injections in [17], where a steady-state analysis is carried out to identify the critical nodes with potential Wobbe index violations. The probabilistic multi-energy flow of IEGS with hydrogen injection is calculated in [18]. The impacts of different hydrogen blending modes on the IEGS are investigated in [19]. In these studies, though the gas compositions across the gas network are evaluated, they cannot be controlled or optimized if security constraints are violated. For example, if the molar fractions of the hydrogen in some parts of the gas network exceed the upper bound, these studies cannot help to provide quantitative suggestions for the IEGS to mitigate the safety issues.

Recently, a few studies focus on the optimal operation of IEGS with alternative gas injections. Compared with the simulation-orientated studies that mainly focus on impact analysis, the optimization-orientated studies focus on decision makings for the system operator of IEGS to improve the operation considering the alternative gas injections. The optimal operation and the aggregated flexibility from multiple power-to-gas units in the IEGS considering the gas composition control are investigated in [20] and [21], respectively. However, in these studies, the optimizations of electricity and gas systems are conducted separately, which cannot coordinate the two energy systems and realize the global optimum. Moreover, the optimal gas flow model with alternative gas is formulated in a nonlinear form and solved by a general nonlinear solver. The computation efficiency and the robustness of the solution can

TABLE I
COMPARISON OF THE MODELS/METHODS PROPOSED IN PREVIOUS STUDIES AND OUR STUDY.

	Proposed in previous studies	Limitations	Proposed in our study	Improvement
Energy flow model	Electricity and gas flow simulation model with alternative gas [9]–[19]	Can not provide corrective suggestions to optimize the IEGS condition	An integrated electricity and gas OEF model with alternative gas	(1) Can provide quantitative suggestions on IEGS operation if some constraints are violated; (2) Electricity and gas systems are fully coordinated to achieve global optimum; (3) The physical characteristics are modeled as variables, so that the impacts of alternative gas can be comprehensively revealed.
	Separate unit commitment model and optimal gas flow model with alternative gas [20], [21], [24]	Electricity and gas systems cannot be well coordinated to reach global optimum		
	OEF models with alternative gas with constant physical characteristicsspecific gravity, compressibility factor, etc. [22], [23]	Impacts of alternative gas on the IEGS cannot be fully revealed		
Solution method	Retain nonlinear form, and is solved by general nonlinear solvers [20], [24]	Computation efficiency and robustness of the solution can not be guaranteed	Well-tailored reformulation techniques and advanced sequential programming method	(1) Original complicated problem is reformulated into a tractable form, so the computation time and robustness of the solution can be improved; (2) Adaptive penalty factors are used to balance the feasibility and convergency; (3) Set security indices as convergence criteria to avoid violation.
	Using commercial solvers by simplifying the OEF model [22], [23]	Oversimplified and may lead to inaccurate solutions		
	Simplify some of the variables and solve it using sequential linear programming [21]	Probable inaccurate solutions, and the convergence may not be guaranteed under extreme cases		

not be guaranteed. In [22], a distributionally robust hydrogen optimization with ensured security and multi-energy couplings is proposed. The volt-VAR-pressure optimization is studied in the distribution-level IEGS in the presence of hydrogen injections in [23]. However, the physical characteristics (including the specific gravity, compressibility factor, etc.) of the natural gas and hydrogen mixtures, are regarded as constants in both studies. By doing so, although the solution of the problem can be simplified, the impacts of alternative gas injection can not be fully revealed. The solution may also be inaccurate and impractical. In [24], the sequential linear programming method is directly used to address the nonlinearities in the gas composition tracking problem. However, convergence may not be well guaranteed under extreme cases due to the intractability of the model.

Concluded from the studies above, the optimal energy flow (OEF) in the IEGS has not been thoroughly modeled for controlling the gas composition with alternative gas injections. The major gaps exist in the coordinated optimization of electricity and gas systems, the modeling of security constraints, and the over-simplification of physical models. The lack of consideration in these aspects can lead to inaccuracies in the OEF calculation. Furthermore, the OEF model with these details is a highly nonlinear optimization problem. The nonlinearity mainly inherits from the Weymouth equation for the gas mixtures, the uncertain gas flow directions, as well as the calculations of security indices, gas composition, specific gravity, compressibility factors, etc. These nonlinearities significantly influence the convergency, accuracy, and computation time of the OEF, which have not been properly handled in previous studies.

To address the research gap, this paper proposes modeling and solution methods for the OEF in the IEGS with alternative gas injections. The contributions are as follows:

(1) An OEF model in IEGS with distributed injections of alternative gases is proposed. Compared with previous studies, 1) the proposed model can fully coordinate the electricity and gas systems to reach the optimal operating condition; 2) the physical characteristics (including the gas composition, specific gravity, compressibility factor, etc.) are modeled as variables, so that the impacts of alternative gases at the nodal scale can be comprehensively revealed and controlled; 3) security indices of gas mixtures in the IEGS, such as the Wobbe index, Weaver flame speed factor, combustion potential, etc., can be evaluated and well contained under varying gas compositions.

(2) Well-tailored reformulation techniques and advanced sequential programming method are developed to solve the nonconvex OEF model. Compared with previous studies, 1) the proposed methods reformulate the original mixed-integer nonlinear programming problem into a more tractable form (mixed-integer second-order-cone (MISOC) programming), and thus the computation efficiency and robustness of the solution can be improved; 2) adaptive penalty factors are used in sequential programming to balance both feasibility and convergency of gas composition constraints, Weymouth equations with varying-parameters, etc; 3) the security indices are set as the convergence criteria, so that the security of the gas system can be better guaranteed.

II. FRAMEWORK OF SECURITY MANAGEMENT WITH ALTERNATIVE GAS INJECTIONS

The structure of the IEGS with the injections of alternative gases is presented in Fig. 1. It consists of electricity and gas systems. In the electricity network, the electricity is supplied from traditional fossil power plants (TPP), GPPs, and renewable generations to satisfy the demand at various locations. In gas systems, multiple types of gases can be injected into the gas network at different locations, including natural gas, biogas, etc., to satisfy the gas demand.

The electricity and gas networks are tightly coupled via GPPs and PTGs. GPPs consume the gas from the gas network to generate electricity. PTGs consume electricity and water to produce hydrogen and methane. The gas products of PTGs need to be purified and compressed first. Then, it can be injected into a private gas network which is separated from the main grid first for security reasons. Due to the sufficient turbulence property in the pipeline, the alternative gas and

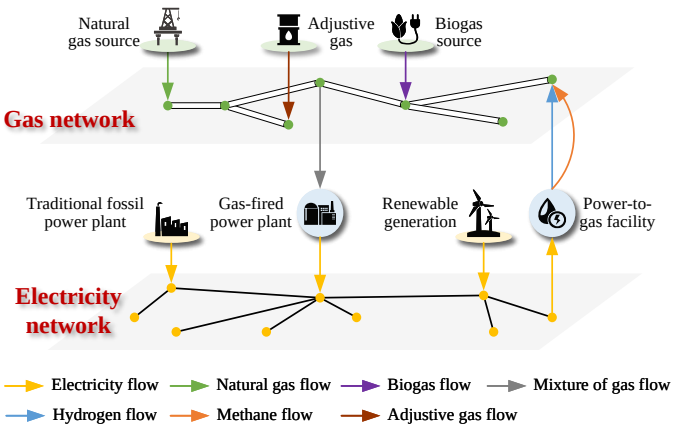

Fig. 1. Structure of the IEGS with the injections of alternative gases.

natural gas can be sufficiently mixed without additional mixing equipment. After the alternative gas is injected into the transmission network, it will be measured at multiple points to ensure the quality of the gas meets expectations. Then, the gas mixtures can be then transported to other locations of the gas systems for further use. The locations of the alternative gas injection depend on many factors, such as the locations of renewable generations, the topology of the gas network, the water supply, etc.

Though blending natural gas with alternative gases may cause security issues, they can be minimized if the quality of the gas mixture is strictly monitored and controlled. Here we mainly focus on the interchangeability of gas. Interchangeability is defined as the ability of the gas mixtures to be consumed by consumers without increasing potential risks or any further adjustment to the gas appliances [12]. Several indices are introduced to ensure the interchangeability of gas:

1) Wobbe index: Wobbe index characterizes the energy output of the gas mixture during combustion under the same pressure. It is a widely used index in many countries such as the UK, Australia, French, etc. [25]. When injecting hydrogen, the Wobbe index of the gas mixture is likely to decrease. Thus, keeping the Wobbe index within a certain range is important for guaranteeing optimal combustion for the gas appliance [26]:

$$GCV_i = \sum_{r\in R} GCV_r x_{i,r} \tag{1}$$

$$WI_i = GCV_i/\sqrt{S_i} \tag{2}$$

where GCV_i is the gross caloric value (GCV) of the gas at bus i; GCV_r is the GCV of the gas component r; $\mathcal{R}$ is the set of gas components; $x_{i,r}$ is the molar fraction of gas component r at bus i; WI_i is the Wobbe index at bus i; S_i is the specific gravity of the gas at bus i.

2) Weaver flame speed factor: Weaver flame speed factor describes the approximate maximum velocity with which a flame can travel in any gas-air mixture. It is also a commonly used index, which is plotted against the Wobbe index to characterize the gas interchangeability by British Gas Corporation. The injection of hydrogen can slightly increase the flame speed [27]. Thus, keeping the Weaver flame speed factor within a certain range is important in avoiding flashbacks, overheating issues, potential corrosion of materials, etc., [28]. It is usually assumed that the maximum flame velocity of a gas mixture is a linear function of each gas component. Then, it can be calculated based on the following empirical equations [29]:

$$FS_i = \frac{\sum_{r\in R} x_{i,r} fs_r}{AF + 5x_i^{\mathrm{N}} - 18.8x_i^{\mathrm{O}} + 1} \tag{3}$$

where FS_i is the Weaver flame speed factor at bus i; fs_r is the burning velocity of gas component r in a stoichiometric air mixture; AF is the air-fuel ratio; x_i^{N} and x_i^{O} are the molar fractions of inert gas component and oxygen at bus i, respectively.

3) Combustion potential: Combustion potential is also a classic and empirical index that measures the interchangeability in terms of the burning rate and combustion stability of natural gas [30]. It is also used as the horizontal axis with the Wobbe index on the vertical axis in the Delbourg method. Keeping combustion potential within a certain range is also important for guaranteeing optimal combustion for gas appliances [5]:

$$CP_i = \sum_{r\in\mathcal{R}} x'_{i,r} CP_{i,r} \sqrt{(S_i/S'_i)} \tag{4}$$

$$x'_{i,r} = x_{i,r}/(1 - x_i^{\mathrm{N}} - x_i^{\mathrm{O}}) \tag{5}$$

$$S'_i = \sum_{r\in\mathcal{R}} x'_{i,r} M_r / \sum_{r\in\mathcal{R}} x_{i,r} M_r \tag{6}$$

$$CP_{i,r} = a_r O_{\mathrm{X}}/\sqrt{S'_{i,r}} \tag{7}$$

where CP_i is the combustion potential at bus i; $x'_{i,r}$ is the correction of $x_{i,r}$ at bus i, which can be calculated as (5); S'_i is the correction of S_i, which can be calculated as (6); $CP_{i,r}$ is the combustion potential for gas component r at bus i, which can be calculated as (7); M_r is the molecular weights of gas component r; a_r is the combustion potential coefficient for gas component r; O_{X} is the oxygen index.

In the proposed OEF model, the molar fraction of hydrogen, specific gravity, and GCV, and above security indices $\boldsymbol{SI}_i = [x_i^{\mathrm{hy}}, S_i, GCV_i, WI_i, FS_i, CP_i]$ should be limited within a certain threshold [6]:

$$|\, \boldsymbol{SI}_i/\boldsymbol{SI}_i^0 - 1 \,| \leq \boldsymbol{\xi}^{\mathrm{SI}} \tag{8}$$

where $\boldsymbol{SI}_i^0$ is the security indices calculated from the original natural gas; $\boldsymbol{\xi}^{\mathrm{SI}}$ is the tolerance for the security indices, which are different in different countries or regions under different conditions [31].

With these indices, the security of the IEGS is regulated mainly by two measures: 1) Regulating the operating condition of PTGs. If gas security is allowed, more hydrogen will be produced by the PTGs and injected into the pipelines. However, due to the lower Wobbe index and higher flame speed factor of hydrogen, excessive injection of hydrogen may cause security issues. Therefore, if the system security is not allowed, the hydrogen production of PTG will be decreased, or more hydrogen will be converted into methane and then injected into the pipelines. 2) Using adjustive gases. The commonly used adjustive gases include nitrogen and liquefied petroleum gas (LPG). LPG has similar gas compositions as

natural gas, and thus it is usually used to neutralize the Wobbe index and GCV decrease by hydrogen. Nitrogen is usually used to regulate flame speed [32]. The adjustive gases are relatively expensive, and thus the cost-benefit usually needs to be considered holistically.

III. OEF Model of IEGS Considering Injection of Alternative Gas

A. Model of the Gas System

1) Model of the gas demand: In the traditional gas system model, the gas demand is usually measured by the gas flow rate at the standard temperature and pressure conditions. This representation is applicable and simplifies the calculation when the gas compositions are the same across the gas network. However, considering the distributed injections of alternative gases, the gas composition varies at different locations in the network. Considering the gas is essentially consumed by gas appliances (e.g., cooking equipment) for combustion to produce heat energy, the gas demand can be represented in the form of energy. The heat energy of the consumed gas mixture should be equivalent to the original gas demand:

$$GCV^{\mathrm{ng}} q_i^{\mathrm{d,ng}} = \sum_{r\in\mathcal{R}} q_{i,r}^{\mathrm{d}} GCV_r,\ q_{i,r}^{\mathrm{d}} \geq 0 \tag{9}$$

$$q_{i,r}^{\mathrm{d}} / \sum_{r\in\mathcal{R}} q_{i,r}^{\mathrm{d}} = x_{i,r} \tag{10}$$

where GCV^{ng} is the GCV of the original natural gas (without blending other gases); $q_i^{\mathrm{d,ng}}$ is the original gas demand; $q_{i,r}^{\mathrm{d}}$ is the demand of gas component r at bus i. It is worth mentioning that all the gas demand or gas flow in this paper is measured by gas flow rate (e.g., Mm^3/day) under standard temperature and pressure condition.

2) Model of the gas source: The gas composition of different gas sources may also vary. Therefore, the gas supply at bus i can be represented by a gas supply vector:

$$\boldsymbol{q}_{i,l}^{\mathrm{s}} = \left[q_{i,l,1}^{\mathrm{s}}, ..., q_{i,l,r}^{\mathrm{s}}, ..., q_{i,l,R}^{\mathrm{s}}\right] \tag{11}$$

$$q_{i,l,r}^{\mathrm{s}} = x_{i,l,r}^{\mathrm{s}} q_{i,l}^{\mathrm{s}},\ \sum_{r\in\mathcal{R}} x_{i,l,r}^{\mathrm{s}} = 1 \tag{12}$$

where $\boldsymbol{q}_{i,l}^{\mathrm{s}}$ is the gas supply vector of gas source l at bus i; R is the number of gas composition; $q_{i,l,r}^{\mathrm{s}}$ is the gas component r supplied by gas source l at bus i; $x_{i,l,r}^{\mathrm{s}}$ is the molar fraction of the gas component r of gas source l at bus i.

The gas production of the gas source should satisfy the upper and lower bounds:

$$\boldsymbol{q}_{i,l}^{\mathrm{s,min}} \leq \boldsymbol{q}_{i,l}^{\mathrm{s}} \leq \boldsymbol{q}_{i,l}^{\mathrm{s,max}} \tag{13}$$

where $\boldsymbol{q}_{i,l}^{\mathrm{s,max}}$ and $\boldsymbol{q}_{i,l}^{\mathrm{s,min}}$ are the upper and lower bounds of the gas supply for gas source l at bus i, respectively. For natural gas sources (gas wells, gas storages, and biogas), the $x_{i,l,r}^{\mathrm{s}}$ take their corresponding values, respectively. If the gas source is LPG, then $x_{i,l,r}^{\mathrm{s}}$ take the values of gas compositions of LPG. If the gas source is nitrogen, then for $r = r^{\mathrm{N}}$, $x_{i,l,r}^{\mathrm{s}} = 1$, otherwise $x_{i,l,r}^{\mathrm{s}} = 0$ (r^{N} is the index for nitrogen).

3) Model of the gas flow in the pipeline: In a transmission pipeline with relatively high gas pressure, the Weymouth equation can be used to describe the relationship between the gas flow rate and nodal gas pressures [33]:

$$q_{i,j}^2 = C_{i,j}^2 (p_i^2 - p_j^2) \tag{14}$$

$$C_{i,j} = \frac{T^{\mathrm{stp}}}{8p^{\mathrm{stp}}} \sqrt{\frac{\pi^2 R^{\mathrm{air}} D_{i,j}^5}{F_{i,j} S_{i,j} L_{i,j} Z_{i,j} T^{\mathrm{gas}}}} \tag{15}$$

$$q_{i,j} = \sum_{r\in\mathcal{R}} q_{i,j,r} \tag{16}$$

$$|q_{i,j}| \leq q_{i,j}^{\max} \tag{17}$$

$$p_i^{\min} \leq p_i \leq p_i^{\max} \tag{18}$$

where $q_{i,j}$ is the gas flow rate between the bus i and j; p_i and p_j are the nodal gas pressure of buses i and j, respectively; $C_{i,j}$ is the property parameter of the pipeline ij; R^{air} is the gas constant of air; T^{stp} and p^{stp} are the temperature and pressure at the standard temperature and pressure conditions, respectively; $D_{i,j}$, $L_{i,j}$, and $F_{i,j}$ are the diameter, length, and friction factor of the pipeline ij, respectively; $S_{i,j}$ and $Z_{i,j}$ are the specific gravity and compressibility factor of the gas mixture in pipeline ij, respectively (note that these two parameters are interdependant on the gas composition in the pipeline, and therefore may be changing during the operation); T^{gas} is the temperature of the gas; $q_{i,j,r}$ is the gas flow rate between the bus i and j for gas component r; $q_{i,j}^{\max}$ is the capacity of the gas pipeline ij; $p_i^{\max}$ and $p_i^{\min}$ are the upper and lower bounds for the nodal gas pressure at bus i, respectively.

4) Nodal balance of gas flow: We assume the mix of gas does not cause any physical or chemical reaction, nor create any state difference in the constituent gases [12]. No gas leak or gas storage effect happens in the gas bus. Then, according to Kirchhoff's law, the gas that flows into a bus is equal to the gas that flows out of the bus for each gas component r:

$$\sum_{l\in\mathcal{L}_i^{\mathrm{s}}} q_{i,l,r}^{\mathrm{s}} - q_{i,r}^{\mathrm{d}} + \sum_{l\in\mathcal{L}_i^{\mathrm{ptg}}} q_{i,l,r}^{\mathrm{ptg}} - \sum_{l\in\mathcal{L}_i^{\mathrm{gpp}}} q_{i,l,r}^{\mathrm{gpp}} - \sum_{j\in\mathcal{J}_i} q_{i,j,r} = 0, \forall r \in \mathcal{R} \tag{19}$$

where $\mathcal{L}_i^{\mathrm{s}}$, $\mathcal{L}_i^{\mathrm{ptg}}$, and $\mathcal{L}_i^{\mathrm{gpp}}$ are the sets of gas sources, PTGs, and GPPs at bus i, respectively; $\mathcal{J}_i$ is the set of bus connected to bus i; $q_{i,l,r}^{\mathrm{ptg}}$ is the gas component r produced by the PTG l at bus i; $q_{i,l,r}^{\mathrm{gpp}}$ is the gas component r consumed by the GPP l at bus i.

5) Model of the gas mixing process: Due to the turbulence in the natural gas flow, the injected hydrogen and natural gas can be mixed uniformly quickly without the help of additional mixing equipment. In the timeframe of our study, the mixing process can be regarded to be finished instantly [34].

On this basis, the mixing process of gases on a single bus is illustrated in Fig. 2. A gas bus can be connected to six kinds of system components. For a specific gas bus, the gases could come from gas sources, PTGs, and upstream pipelines. These gases are fully mixed uniformly at the gas bus, and then the gas mixture is transported to gas loads, GPPs, and downstream pipelines. To describe the gas mixing process, we denote the sum of gas component r that flows into the gas bus i as $W_{i,r}$, and denote the sum of all gas components that flows

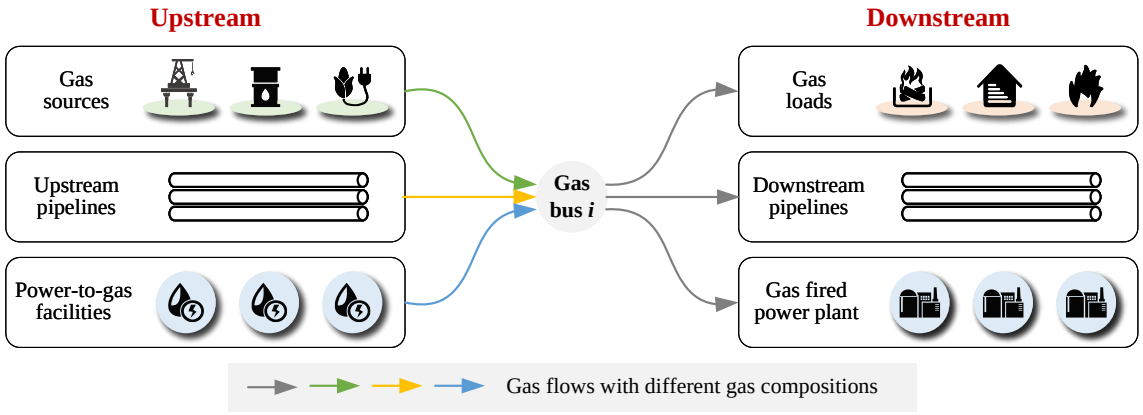

Fig. 2. Illustration of the nodal gas mixing process.

into the gas bus i as W_i ($W_i = \sum_{r\in\mathcal{R}} W_{i,r}$). They are all measured in gas flow rate (Mm^3/day) in standard temperature and pressure conditions. Because the nodal gas injection is related to the direction of gas flow in the pipeline, and the direction may change under different conditions, the actual gas flow direction is described by an integer variable $\gamma_{i,j} \in \{-1, 1\}$, where $\gamma_{i,j} = 1$ indicates that the gas flows from bus i to j, and $\gamma_{i,j} = -1$ indicates otherwise. Then, the nodal gas injection for component r can be calculated by:

$$W_{i,r} = \sum_{j\in\mathcal{J}_i} \frac{\gamma_{i,j}-1}{2} q_{i,j,r} + \sum_{l\in\mathcal{L}_i^{\mathrm{s}}} q_{i,l,r}^{\mathrm{s}} + \sum_{l\in\mathcal{L}_i^{\mathrm{ptg}}} q_{i,l,r}^{\mathrm{ptg}} \tag{20}$$

The gas composition at bus i can be calculated by:

$$x_{i,r} = W_{i,r}/W_i,\ W_i = \sum_{r\in\mathcal{R}} W_{i,r} \tag{21}$$

In (14), the specific gravity and compressibility factor are variables, which are determined by the gas composition in the exact pipeline. They can be calculated as [35]:

$$S_i = \sum_{r\in\mathcal{R}} M_r x_{i,r}/M^{\mathrm{air}} \tag{22}$$

$$S_{i,j} = \left((1+\gamma_{i,j})S_i + (1-\gamma_{i,j})S_j\right)/2 \tag{23}$$

$$Z_{i,j} = f_Z(\boldsymbol{x}_i, \boldsymbol{x}_j, p_i, p_j) \tag{24}$$

where M^{air} is the molecular weights of air; f_Z is the function of compressibility factor with respect to the gas compositions and nodal gas pressures, the details of which are elaborated in Appendix.

Remark 1. *In the traditional Weymouth equation in (14)-(15), the specific gravity and compressibility factor are constants. However, after considering the injection of alternative gases, the gas composition is varying across the gas network. Thus, the specific gravity and compressibility factor are also optimization variables in the OEF model, as calculated in (22)-(24). Compared with previous studies [22], [23], the Weymouth equation becomes more nonconvex, but the impacts of alternative gas injection can be characterized more accurately.*

B. Model of the Coupling Components

1) PTG facility: PTG facilities usually consume surplus renewable generations to produce gas. This process consists of two sequential subprocesses, namely, electrolysis and methanation, which produce hydrogen and methane, respectively. The relationship between electricity consumption and gas production can be represented by:

$$P_{i,l}^{\mathrm{ptg}}\eta_{i,l}^{\mathrm{e}} = q_{i,l}^{\mathrm{hy}} GCV^{\mathrm{hy}} + q_{i,l}^{\mathrm{me}} GCV^{\mathrm{me}}/\eta_{i,l}^{\mathrm{me}} \tag{25}$$

$$q_{i,l}^{\mathrm{ptg}} = \sum_{r\in\mathcal{R}} q_{i,l,r}^{\mathrm{ptg}} = q_{i,l}^{\mathrm{hy}} + q_{i,l}^{\mathrm{me}},\ q_{i,l}^{\mathrm{hy}} \geq 0, q_{i,l}^{\mathrm{me}} \geq 0 \tag{26}$$

where $P_{i,l}^{\mathrm{ptg}}$ is the electricity consumed by PTG l at bus i; $\eta_{i,j}^{\mathrm{e}}$ and $\eta_{i,l}^{\mathrm{me}}$ are the efficiencies of electrolysis and methanation processes, respectively; GCV^{hy} and GCV^{me} are the GCVs of methane and hydrogen, respectively; $q_{i,l}^{\mathrm{hy}}$ and $q_{i,l}^{\mathrm{me}}$ are the hydrogen and methane productions of PTG l at bus i, respectively.

The electricity consumption of PTG is further limited by:

$$0 \leq P_{i,l}^{\mathrm{ptg}} \leq P_{i,l}^{\mathrm{ptg,max}} \tag{27}$$

where $P_{i,l}^{\mathrm{ptg,max}}$ is the maximum electricity consumption of the PTG l at bus i.

2) GPP: GPPs consume gas mixtures to produce electricity, which can be represented by:

$$P_{i,l}^{\mathrm{gpp}} = \eta_{i,l}^{\mathrm{gpp}} \sum_{r\in\mathcal{R}} q_{i,l,r}^{\mathrm{gpp}} GCV_r,\ q_{i,l,r}^{\mathrm{gpp}} \geq 0 \tag{28}$$

$$q_{i,l,r}^{\mathrm{gpp}} / \sum_{r\in\mathcal{R}} q_{i,l,r}^{\mathrm{gpp}} = x_{i,r} \tag{29}$$

where $P_{i,l}^{\mathrm{gpp}}$ is the electricity generation of GPP l at bus i; $\eta_{i,l}^{\mathrm{gpp}}$ is the efficiency of the GPP l; $q_{i,l,r}^{\mathrm{gpp}}$ is the gas component r consumed by the GPP l.

C. Model of the Electricity System

AC power flow is used to model the electricity system. Second-order-cone (SOC) relaxation is also employed to convexify the AC power flow model [36]:

$$\begin{aligned} &\sum_{l\in\mathcal{L}_i^{\mathrm{tpp}}} P_{i,l}^{\mathrm{tpp}} + \sum_{l\in\mathcal{L}_i^{\mathrm{gpp}}} P_{i,l}^{\mathrm{gpp}} + \sum_{l\in\mathcal{L}_i^{\mathrm{rng}}} P_{i,l}^{\mathrm{rng}} \\ &- \sum_{l\in\mathcal{L}_i^{\mathrm{ptg}}} P_{i,l}^{\mathrm{ptg}} - P_i^{\mathrm{d}} - \sum_{j\in\mathcal{J}_i} P_{i,j} = 0 \\ &\sum_{l\in\mathcal{L}_i^{\mathrm{tpp}}} Q_{i,l}^{\mathrm{tpp}} + \sum_{l\in\mathcal{L}_i^{\mathrm{gpp}}} Q_{i,l}^{\mathrm{gpp}} + \sum_{l\in\mathcal{L}_i^{\mathrm{rng}}} Q_{i,l}^{\mathrm{rng}} \end{aligned} \tag{30}$$

$$-\sum_{l\in\mathcal{L}_i^{\text{ptg}}} Q_{i,l}^{\text{ptg}} - Q_i^d - \sum_{j\in\mathcal{J}_i} Q_{i,j} = 0 \tag{31}$$

$$V_i - V_j = 2(R_{i,j}P_{i,j} + X_{i,j}Q_{i,j}) - (R_{i,j}^2 + X_{i,j}^2)I_{i,j} \tag{32}$$

$$V_i I_{i,j} \geq (P_{i,j})^2 + (Q_{i,j})^2 \tag{33}$$

$$||P_{i,j}, Q_{i,j}||_2 \leq SL_{i,j}^{\max} \tag{34}$$

$$P_{i,l}^{\text{tpp,min}} \leq P_{i,l}^{\text{tpp}} \leq P_{i,l}^{\text{tpp,max}},\ Q_{i,l}^{\text{tpp,min}} \leq Q_{i,l}^{\text{tpp}} \leq Q_{i,l}^{\text{tpp,max}} \tag{35}$$

$$P_{i,l}^{\text{gpp,min}} \leq P_{i,l}^{\text{gpp}} \leq P_{i,l}^{\text{gpp,max}},\ Q_{i,l}^{\text{gpp,min}} \leq Q_{i,l}^{\text{gpp}} \leq Q_{i,l}^{\text{gpp,max}} \tag{36}$$

$$P_{i,l}^{\text{rng,min}} \leq P_{i,l}^{\text{rng}} \leq P_{i,l}^{\text{rng,max}},\ Q_{i,l}^{\text{rng,min}} \leq Q_{i,l}^{\text{rng}} \leq Q_{i,l}^{\text{rng,max}} \tag{37}$$

$$Q_{i,l}^{\text{rng,max}} \leq \tan(\arccos(\phi_{i,l})) \tag{38}$$

$$V_i^{\min} \leq V_i \leq V_i^{\max} \tag{39}$$

where (30) and (31) are the active and reactive nodal electricity balance constraints, respectively; (32) represents the relation between the voltage drop and electricity flow in an electricity branch; (33) is the SOC relaxation constraint; (34) is the upper bounds for apparent power flow in an electricity branch; (35) - (37) are the upper and lower bounds for active and reactive power outputs of TPPs, GPPs, and renewable generations, respectively; (38) defines the maximum reactive power output of renewable generators; (39) is the bounds for voltage magnitude; $\mathcal{L}_i^{\text{tpp}}$ and $\mathcal{L}_i^{\text{rng}}$ are the sets of TPPs and renewable generators at bus i, respectively; $P_{i,l}^{\text{gpp}}$, $P_{i,l}^{\text{tpp}}$, $P_{i,l}^{\text{rng}}$, and $P_{i,l}^{\text{ptg}}$ are the active powers of electricity generations of GPP, TPP, and renewable generator l at bus i, respectively; P_i^{d} is the active power of electricity demand at bus i; $P_{i,j}$ is the active power of the electricity flow on branch i,j; $Q_{i,l}^{\text{gpp}}$, $Q_{i,l}^{\text{tpp}}$, $Q_{i,l}^{\text{rng}}$, and $Q_{i,l}^{\text{ptg}}$ are the reactive powers of electricity generations of GPP, TPP, renewable generator, and PTG l at bus i, respectively; Q_i^{d} is the reactive power of electricity demand at bus i; $Q_{i,j}$ is the reactive power of the electricity flow on branch i,j; V_i is the square of voltage magnitude at bus i; $I_{i,j}$ is the square of current magnitude of branch i,j; $R_{i,j}$ and $X_{i,j}$ are the resistance and reactance of branch ij, respectively; $SL_{i,j}^{\max}$ is the apparent capacity of branch i,j; $P_{i,l}^{\text{tpp,max}}$, $P_{i,l}^{\text{tpp,min}}$, $P_{i,l}^{\text{gpp,max}}$, $P_{i,l}^{\text{gpp,min}}$, $P_{i,l}^{\text{rng,max}}$, and $P_{i,l}^{\text{rng,min}}$ are the upper and lower bounds of the active power outputs of TPPs, GPPs, and renewable generators, respectively; $Q_{i,l}^{\text{tpp,max}}$, $Q_{i,l}^{\text{tpp,min}}$, $Q_{i,l}^{\text{gpp,max}}$, $Q_{i,l}^{\text{gpp,min}}$, $Q_{i,l}^{\text{rng,max}}$, and $Q_{i,l}^{\text{rng,min}}$ are the upper and lower bounds of the reactive power outputs of TPPs, GPPs, and renewable generators, respectively; $\phi_{i,l}$ is the power factor of renewable generator l at bus i.

D. Objective Function

The objective of the OEF is to minimize the total operating cost C^T by regulating the operating conditions of the IEGS components (i.e., TPPs, GPPs, renewable generators, PTGs, and gas sources). The operating cost includes the electricity generation cost of TPPs, the gas production cost of gas sources, and the subsidy from the green hydrogen productions:

$$\begin{aligned} C^{\text{T}} = &\sum_{i\in\mathcal{I}} \sum_{l\in\mathcal{L}_i^{\text{gpp}}} cst_{i,l}(P_{i,l}^{\text{tpp}}, Q_{i,l}^{\text{tpp}}) \\ &+ \sum_{i\in\mathcal{I}} \rho_{i,l}^{\text{s}} q_{i,l}^{\text{s}} + \mu \sum_{i\in\mathcal{I}} \sum_{l\in\mathcal{L}_i^{\text{ptg}}} q_{i,l}^{\text{ptg}} \end{aligned} \tag{40}$$

where $\mathcal{I}$ is the set of buses; $cst_{i,l}$ is the cost function of TPP l at bus i; $\rho_{i,l}^{\text{s}}$ is the nodal price for the gas production of gas source l at bus i; μ is the subsidy price for the green gas production.

IV. Reformulation of OEF Model

The above OEF model in Section III is highly nonlinear and nonconvex, which can not be solved directly by using the off-the-shelf solvers. The nonlinear terms in the OEF model take various forms, and different reformulation techniques should be applied.

A. MISOC Relaxation of Gas Flow Equations

The nonlinear Weymouth equation for gas mixtures in (14) can be converted into an MISOC form [37]:

$$\Phi_{i,j} \geq \Theta_{i,j} S_{i,j} Z_{i,j} q_{i,j}^2 \tag{41}$$

$$\Phi_{i,j} \geq p_j^{\text{s}} - p_i^{\text{s}} + (\gamma_{i,j}+1)(p_i^{\text{s,min}} - p_j^{\text{s,max}}) \tag{42}$$

$$\Phi_{i,j} \geq p_i^{\text{s}} - p_j^{\text{s}} + (\gamma_{i,j}-1)(p_i^{\text{s,max}} - p_j^{\text{s,min}}) \tag{43}$$

$$\Phi_{i,j} \leq p_j^{\text{s}} - p_i^{\text{s}} + (\gamma_{i,j}+1)(p_i^{\text{s,max}} - p_j^{\text{s,min}}) \tag{44}$$

$$\Phi_{i,j} \leq p_i^{\text{s}} - p_j^{\text{s}} + (\gamma_{i,j}-1)(p_i^{\text{s,min}} - p_j^{\text{s,max}}) \tag{45}$$

where $\Theta_{i,j} = \frac{64(p^{stp})^2 F_{i,j} L_{i,j} T^{gas}}{(T^{stp})^2 \pi^2 R^{air} D_{i,j}^5}$; $\Phi_{i,j}$ is an auxiliary variable for pipeline ij; $p_i^{\text{s}} = p_i^2$ is the square of nodal pressure; $p_i^{\text{s,min}} = (p_i^{\text{s,min}})^2$ and $p_i^{\max} = (p_i^{\max})^2$. Equations (17) and (18) are replaced by (46) and (47), respectively:

$$(\gamma_{i,j}-1)q_{i,j}^{\min}/2 \leq q_{i,j} \leq (\gamma_{i,j}+1)q_{i,j}^{\max}/2 \tag{46}$$

$$p_i^{\text{s,min}} \leq p_i^{\text{s}} \leq p_i^{\text{s,max}} \tag{47}$$

However, the relaxation of (41)-(47) is not always exact. To drive the relaxation tight, two techniques, namely, penalty function and sequential cone programming are adopted:

1) In the penalty function method, to drive (41) tight, a penalty term $\lambda\Phi_{i,j}$ is added to the objective in (40), where λ is the penalty coefficient. The specific procedure will be introduced in detail in Section V. This method can drive the relaxation tight without increasing the computation burden. However, the penalty coefficient is difficult to select in practical cases to balance the penalty with the original objective. An excessively large penalty factor may trigger numerical problems, while a small value of the penalty factor may cause a certain level of inexactness. Therefore, the sequential cone programming technique is further utilized.

2) In the sequential cone programming, the idea is to update the feasible region of the optimization problem with each iteration. This method allows the optimization problem to be tentatively solved at first with certain violations of constraints, while it gradually approaches the true feasible region as the iteration proceeds. Although this method may increase a certain level of computation time, the solution process will be more robust and easy to converge [38], [39]. Correspondingly, an additional constraint based on Taylor approximation is added to make (41) tight:

$$\Phi_{i,j} \leq \Theta_{i,j} S_{i,j}^{(v)} Z_{i,j}^{(v)} \left((q_{i,j}^{(v)})^2 + 2q_{i,j}^{(v)}(q_{i,j} - q_{i,j}^{(v)}) \right)$$

$$+\sigma_{i,j}^{\Phi,(v)},\ \sigma_{i,j}^{\Phi,(v)} \geq 0 \quad (48)$$

where v is the index for iteration; $\Phi_{i,j}^{(v)}$ represents the value of $\Phi_{i,j}$ at the v-th iteration; $\sigma_{i,j}^{\Phi,(v)}$ is the slack variable representing the error of Taylor approximation of $\Phi_{i,j}^{(v)}$. (41) can be handled similarly. The detailed procedures of the sequential cone programming will be introduced in Section V.

B. Reformulation of Bilinear Terms Using McCormick Envelopes

The bilinear terms exist in the gas mix equation and calculation of specific gravity in (20)-(23). We can observe from these equations that the bilinear term is composed of an integer variable and a continuous variable. Therefore, the relaxation using the McCormick envelopes can be exact [40].

Firstly, equations (20)-(21) can be equivalent to the following constraints by using Taylor approximation:

$$x_{i,r}^{(v)} = x_{i,r}^{(v-1)} + \Delta W_{i,r}^{(v)}/W_i^{(v-1)} + \varepsilon_{i,r}^{x,(v)} \quad (49)$$

$$-\sigma_{i,r}^{x,(v)} \leq \varepsilon_{i,r}^{x,(v)} \leq \sigma_{i,r}^{x,(v)},\ \sigma_{i,r}^{x,(v)} \geq 0 \quad (50)$$

where $\Delta W_{i,r}^{(v)}$ is the increment of $W_{i,r}$ in the v-th iteration; $\varepsilon_{i,r}^{x,(v)}$ is the slack variable, which represents the Taylor remainder for the gas composition at bus i for gas component r in the v-th iteration; $\sigma_{i,r}^{x,(v)}$ is the upper bound for $\varepsilon_{i,r}^{x,(v)}$, which is used to drive (49) tight. It should be noted that the reference point of $\Delta W_{i,r}^{(v)}$ in the Taylor approximation is selected according to the value in the last iteration $v-1$. Therefore, it can also be handled by the sequential programming technique.

Then, let $\omega_i = \frac{\gamma_{i,j}+1}{2} x_{i,r}$, (23) can be replaced by using the McCormick envelopes:

$$S_{i,j} = \left(\sum_{r\in\mathcal{R}} M_r \omega_{i,r} - \sum_{r\in\mathcal{R}} M_r (\omega_{j,r} + x_{j,r}) \right) / M^{\text{air}} \quad (51)$$

$$0 \leq \omega_{i,r} \leq x_{i,r} \quad (52)$$

$$\omega_{i,r} \leq (\gamma_{i,j}+1)/2 \quad (53)$$

$$\omega_{i,r} \geq (\gamma_{i,j}+1)/2 + x_{i,r} - 1 \quad (54)$$

C. Linearization of Security Indices

For the Wobbe index in (2), the nonlinear terms exist in the form of $\sqrt{S_i}$. Taking the original gas specific gravity S^{ng} as the reference point, it can be linearized using Taylor approximation:

$$\sqrt{S_i} = \frac{1}{2}\left(\frac{S_i}{\sqrt{S^{\text{ng}}}} + \sqrt{S^{\text{ng}}} \right) \quad (55)$$

Substitute (55) into (2), and the linear form can be obtained.

In addition, we assume the proportions of oxygen and nitrogen are constants in the gas network. With this assumption, the equations for both the Weaver flame speed factor in (3) and combustion potential indices (4) can be linearized.

V. Solution Procedure Using Sequential Programming

After reformulations and relaxations in Section III, the original highly nonlinear OEF optimization problem has been converted into a MISOC programming problem. However, some of the relaxations are not tight. Therefore, advanced sequential programming is devised with self-adaptive penalty factors to improve convergency and computation efficiency. The solution procedure is elaborated as follows:

Step 1: Initialize the physical parameters of the IEGS, security constraints, and other related parameters.

Step 2: Solve the OEF problem in the IEGS without the injection of alternative gas [41]. Obtain the solutions as the reference point.

Step 3: Initialize the iteration index $v = 0$. Initialize the reference points of the sequential programming according to the solutions in **Step 2**, including $q_{i,j,r}^{(0)}$, $x_{i,r}^{(0)}$, $\gamma_{i,j}^{(0)}$, $q_{i,l}^{\text{s},(0)}$, $q_{i,l}^{\text{ptg},(0)}$, $W_i^{(0)}$, $W_{i,r}^{(0)}$, $S_{i,j}^{(0)}$, and $Z_{i,j}^{(0)}$. Initialize the penalty factors for sequential programming $\alpha^{\Phi,(0)}$, $\alpha^{x,(0)}$ and their upper bounds $\alpha^{\Phi,\max}$, $\alpha^{\text{x},\max}$. Set the residual tolerances ϵ^{Φ}, ϵ^{x},ϵ^{f}, ϵ^{S}, and ϵ^{Z}.

Step 4: In the the v-th iteration, solve the following MISOC programming problem:

$$\min \quad f^{(v)} = C^{\text{T}} + \sum_{(i,j)\in\mathcal{GP}} \left(\lambda \Phi_{i,j} + \alpha^{\Phi,(v)} \sigma_{i,j}^{\Phi,(v)} \right) + \sum_{i\in\mathcal{I}} \alpha^{\text{x},(v)} \sigma_{i,r}^{\text{x},(v)} \quad (56)$$

subject to: (9)-(13), (19), (25)-(8), (41)-(54). $\mathcal{GP}$ is the set of gas pipelines. It should be noted that the term $\sqrt{S_i}$ in the security constraint is replaced by (55). The optimization variables can be selected as: 1) square of the nodal gas pressure P_i; 2) gas production of gas source $q_{i,l}^{\text{s}}$; 3) gas demand for each gas component $q_{i,r}^{\text{d}}$; 4) hydrogen and methane productions of PTG $q_{i,l}^{\text{hy}}$ and $q_{i,l}^{\text{me}}$; 5) electricity consumption of PTG $g_{i,l}^{\text{ptg}}$; 6) electricity generations of TPP $g_{i,l}^{\text{tpp}}$, GPP $g_{i,l}^{\text{gpp}}$, and renewable generators $g_{i,l}^{\text{rng}}$; 7) gas comsumption of gas component r for GPPs $q_{i,l,r}^{\text{gpp}}$; 8) phase angle of the voltage θ_i; 9) direction of gas flow $\gamma_{i,j}$; 10) gas composition $x_{i,r}$; 11) gas flow for each gas component in the pipeline $q_{i,j,r}$; 12) auxiliary variables $\Phi_{i,j}$, $\sigma_{i,j}^{\Phi}$, $\varepsilon_{i,r}^{\text{x}}$, $\sigma_{i,r}^{\text{x}}$, and $\omega_{i,r}$. Solve the above optimization problem and obtain the solution for the v-th iteration.

Step 5: Update the $W_{i,r}^{(v)}$, $S_{i,j}^{(v)}$, and $Z_{i,j}^{(v)}$ in this iteration according to (20), (23), and (24), respectively.

Step 6: Check if the residuals of the sequential programming are within the tolerances:

$$\left[\sum_{(i,j)\in\mathcal{GP}} \sigma_{i,j}^{\Phi,(v)}, \sum_{r\in\mathcal{R}} \sum_{i\in\mathcal{I}} \sigma_{i,r}^{\text{x},(v)}, |f^{(v)} - f^{(v-1)}|, \sum_{(i,j)\in\mathcal{GP}} |S_{i,j}^{(v)} - S_{i,j}^{(v-1)}|, \sum_{(i,j)\in\mathcal{GP}} |Z_{i,j}^{(v)} - Z_{i,j}^{(v-1)}| \right] \leq [\epsilon^{\Phi}, \epsilon^{\text{x}}, \epsilon^{\text{f}}, \epsilon^{\text{S}}, \epsilon^{\text{Z}}] \quad (57)$$

If the above inequality holds, the sequential programming ends, and outputs the final results. Otherwise, update the penalty factor as follows, and repeat from **Step 4**.

$$\alpha^{\Phi,(v+1)} = \min\left\{ \kappa \alpha^{\Phi,(v)}, \alpha^{\Phi,\max} \right\} \quad (58)$$

$$\alpha^{\text{x},(v+1)} = \min\left\{ \kappa \alpha^{\text{x},(v)}, \alpha^{\text{x},\max} \right\} \quad (59)$$

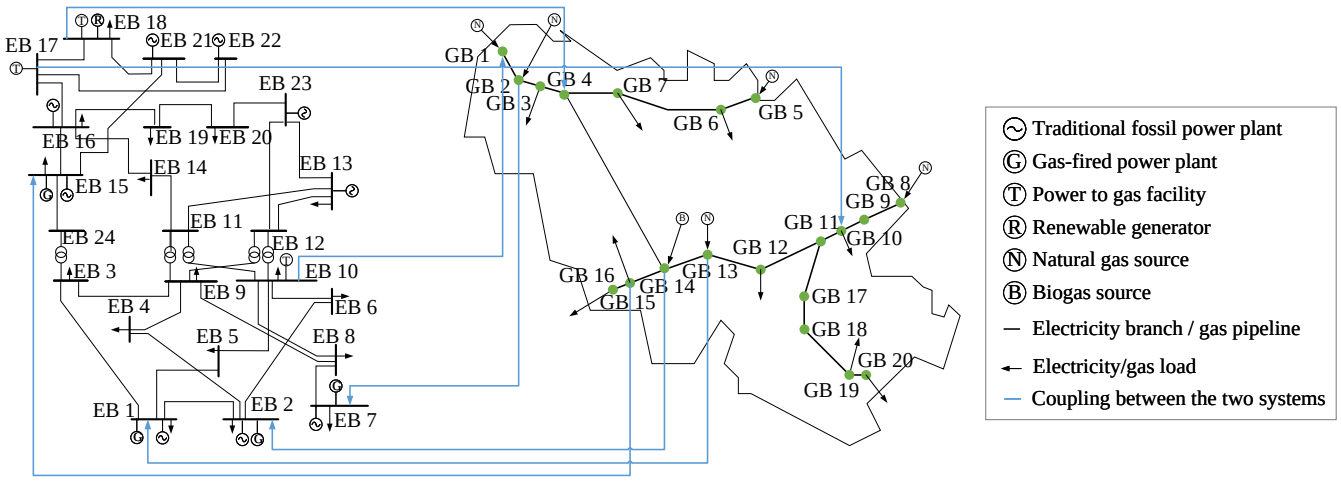

Fig. 3. The test IEGS composed by IEEE 24 bus RTS and Belgium gas transmission system.

TABLE II
GAS COMPOSITIONS OF GAS SOURCES

Gas component	Fraction of the gas component of the gas source					
	#1 (GB 1)	#2 (GB 2)	#3 (GB 5)	#4 (GB 8)	#5 (GB 13)	#6 (GB 14)
Methane	91.92	86.28	91.66	92.19	97.71	94.00
Ethane	4.39	7.01	3.88	4.32	0.63	0.00
Propane	0.53	1.21	0.46	0.43	0.07	0.00
I-butane	0.09	0.27	0.13	0.03	0.02	0.00
Hydrogen	0.00	0.00	0.00	0.00	0.00	0.50
Nitrogen	0.76	0.50	1.54	0.76	1.12	2.50
Carbon dioxide	2.31	4.73	2.33	2.28	0.45	2.50

where κ is the multiplier of penalty factors.

VI. CASE STUDIES

An IEGS test case, composed by IEEE 24 bus RTS [42] and Belgium gas transmission system [43], is used to validate the effectiveness of the modeling and solution methods in this paper [44], [45]. Following modifications are made to the original systems: 1) the two energy systems are topologically coupled according to Fig. 3; 2) the generator # 1, 2, 5, 6, 9-11, and 16-20 are replaced with GPPs (the index of the generator can be found in [42]); 3) the hydrogen production capacities of PTGs are set to 0.5 Mm^3/day; 4) the gas compositions of gas sources are different, as presented in Table I [12], [20]. The optimization problem is solved using Mosek solver, which is performed on a laptop with Intel(R) Core(TM) i7-8565U CPU @1.80GHz and 16 GB RAM.

A. Effectiveness of the Proposed Solution Methods

In this section, the effectiveness of the proposed solution methods is validated. The convergence curve of the sequential programming is presented in Fig. 4. The relative errors of auxiliary variables for gas flow, gas composition, operating cost, specific gravity, and compressibility factor are converged to less than 10^{-1} after 8 iterations. The corresponding computation time is 1.30s. After 10 iterations, the relative errors are further reduced to 10^{-2}, and the computation time is 1.47s. It validates that the proposed sequential programming converges quickly, and is computationally efficient.

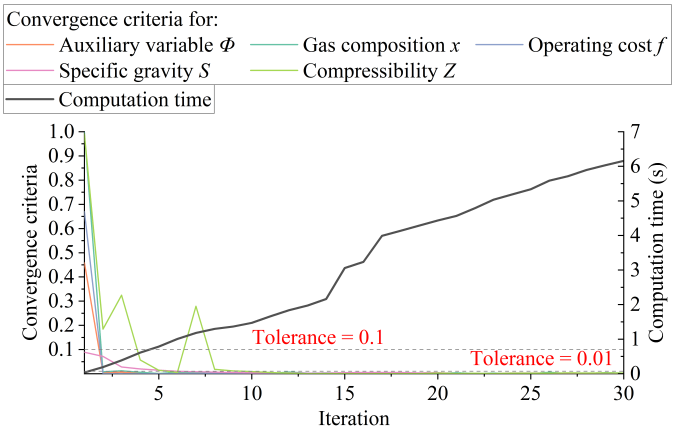

Fig. 4. Convergence and computation time of the proposed solution methods.

TABLE III
COMPARISON OF DIFFERENT BENCHMARK METHODS

	Method A	Method B	Method C	Method D
Computation time (s)	1.47	1.23	3381	41.36
Relative error of gas composition to Method D (%)	1.57×10^{-2}	4.66×10^{-2}	6.16×10^{-3}	/
Relative error operating cost to Method D (%)	9.31×10^{-4}	3.01×10^{-1}	3.13×10^{-5}	/

To validate the credibility of the optimization results, the proposed method is compared with three other benchmark methods. Method A is the proposed method. In method B, piecewise linear functions are used to approximate the original nonlinear constraints. Then, the original problem is transferred into a mixed-integer linear programming problem. In method C, the Gurobi solver is used, which uses branch&cut and McCormick envelope to handle the bilinear terms. In method D, the optimization model stays nonlinear, and is solved using the BONMIN solver.

The four methods are compared in Table. III. We can see that the proposed method is more balanced between the computation time and accuracy. Though it is 19.51% slower than method B, its relative errors in terms of gas composition and operating cost are 66.31% and 99.69% smaller, respectively. The relative errors of different methods are presented in detail in Fig. 5. Except for several buses, the relative errors in the

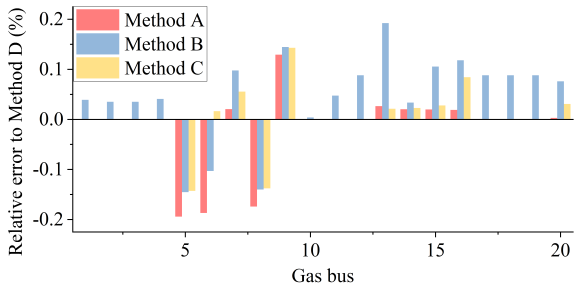

Fig. 5. Relative error of different methods at gas buses

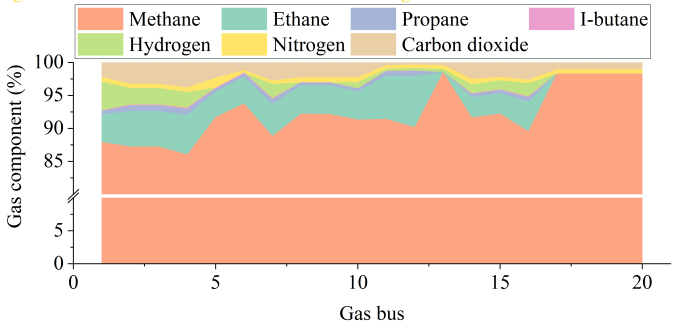

(a) Nodal gas compositions.

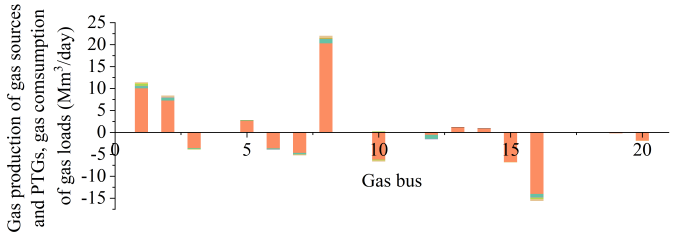

(b) Nodal gas productions of gas sources and PTGs, and nodal gas consumptions of gas loads.

Fig. 6. Optimization results of gas compositions and nodal injections.

proposed method (Method A) are all smaller than in other methods. Although method C presented a smaller average error compared with method B, its computation time is much higher. Compared with method D, the proposed method also presents a higher efficiency. The computation time can be reduced by 96.44%.

B. Optimization Results of the OEF in IEGS With Injections of Alternative Gases

The OEF results are shown first in this section. The nodal gas compositions, gas productions of gas sources and PTGs, and gas consumptions of gas loads are shown in Fig. 6. It can be observed that the gas compositions vary in different buses, which are influenced by the injections of alternative gases. For example, due to the 0.5 Mm^3/day hydrogen production from the PTG, the molar fraction of hydrogen at bus 1 is the highest at 4.36%. Due to the 0.22 Mm^3/day hydrogen injection into bus 10, the molar fraction increases slightly.

The security indices are presented in Fig. 7. It can be seen that all the security indices are controlled smoothly within the security range. The deviations of the four security indices at each bus are limited to 8.76%, 8.99%, 5.66%, and 6.58%, respectively. The slight variations of security indices at different

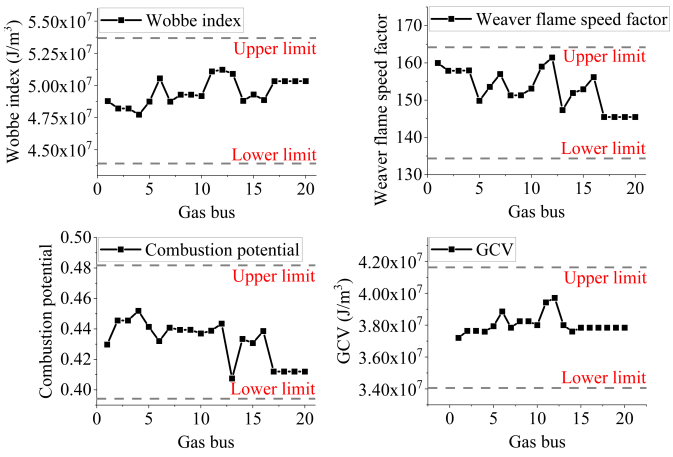

Fig. 7. Nodal security indices.

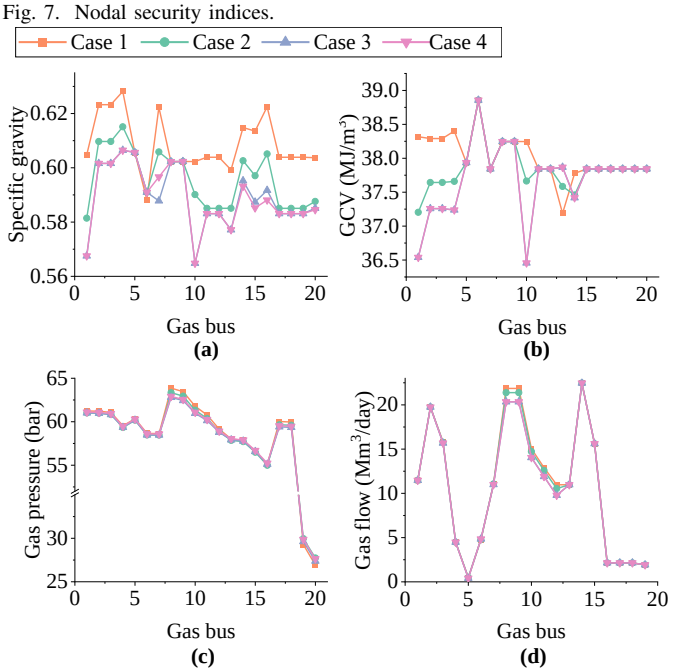

Fig. 8. Impacts of gas composition variations on the physical characteristics: (a) specific gravity; (b) GCV; (c) gas pressure; (d) gas flow.

buses are caused by the fluctuations in gas compositions. For example, the Wobbe index at bus 12 is higher than the original natural gas due to the increased molar fraction of ethane.

To investigate the impacts of different levels of alternative gas injections on the physical parameters (e.g., specific gravity) of the gas mixture, and the impacts of varying physical parameters on the operation of IEGS, four cases are set. The upper and lower bounds of security indices, including the molar fraction of hydrogen, Wobbe Index, etc., are relaxed to ±20% to allow sufficient alternative gas injections. The gas production capacities of PTGs in Cases 1, 2, 3, and 4 are set to 0, 0.5, 2, and 5 Mm^3/day, respectively. The specific gravity, GCV, and gas pressure at each bus, and the gas flow at each gas pipeline are presented in Fig. 8.

From Fig. 8.(a) and Fig. 8.(b), we can find that the alternative gas injection will significantly decrease the specific gravity and GCV of gas mixtures. For example, the average nodal specific gravity of Cases 2, 3, and 4 are 2.13%, 3.22%, and 3.23% lower than Case 1, respectively. The alternative gas injection also causes variations in the nodal gas pressures and

TABLE IV
COMPARISON OF IEGS CONDITIONS WITH DIFFERENT ADJUSTIVE GASES

	Case 5	Case 6	Case 7	Case 8
PTG capacity (Mm^3/day)	0.5	2	2	2
Boundaries of security indices	±5%	±5%	±10%	±5%
Relative cost of adjustive gas to other gas sources	1.5	1.5	1.5	3
Gas production of PTGs (Mm^3/day)	1.031	1.504	2.467	1.369
Injection of adjustive gas (Mm^3/day)	0.307	0.342	0.025	0.125
Adjustive gas cost ($)	3.92×10^4	4.36×10^4	1.30×10^2	1.32×10^3
Total cost ($)	4.14×10^6	3.96×10^6	3.77×10^6	3.98×10^6

gas flows. For example, the difference of the gas pressures at gas bus #8 and #20 in Case 1 is 4.32% higher than in Case 4. This is because the gas in Case 1 has a higher specific gravity, which requires a higher gas pressure difference to transport the same amount of gas. It is also worth noting that the presented differences in IEGS conditions with different levels of alternative gas have already been mitigated by using the proposed OEF technique. If we do not optimize the IEGS with the OEF method, the impacts of alternative gas injection will be even more significant [12].

C. Applications of the Proposed OEF Model

In this subsection, to demonstrate the application of the proposed OEF method, seven comparative groups are set to conduct different impact analyses on the IEGS operating condition with alternative gas.

1) Comparison of AC and DC power flow models: The differences in the IEGS operating conditions with/without considering detailed security constraints of electricity systems are shown in Fig. 9. As we can see, the gas compositions with DC and AC models are almost the same, with an average difference of 0.28%. The situations are similar with gas pressures and gas productions. The average differences between the AC and DC models are 0.47% and 1.11%, respectively. However, the situation for the power output of generators is a little different. Most of the generators' active powers are similar, except for generators #13, 23, and 24. This is because the transmission capacities of electric branches are relatively redundant in the test system. In the DC power flow model, the allocation of power output mainly depends on the generating cost. Generators #23 and 24 are all renewable generators with low marginal costs. Therefore, the allocation of power output between the two renewable generators is relatively stochastic during the solution of the optimization problem. While in the AC power flow model, other factors, such as line loss, reactive power, etc., will affect the generations. Therefore, the allocation of power is different from that in the DC model.

2) Tech-economic analysis of using adjustive gas: To investigate the benefit of using adjustive gases, four cases are set, as shown in Table. IV. The gas sources of both LPG and nitrogen are added to the gas buses where the alternative gases are injected, i.e., gas bus #1, 4, and 10. The gas compositions of adjustive gases can be found in [22].

Comparing Cases 5 and 6, we can see that the increase in PTG capacity leads to more alternative gas injections, and requires more adjustive gases. The adjustive gas cost in Case 6 is 11.22% higher than in Case 5, while the total cost in Case 6 is 4.35% lower than in Case 5. This indicates when the unit

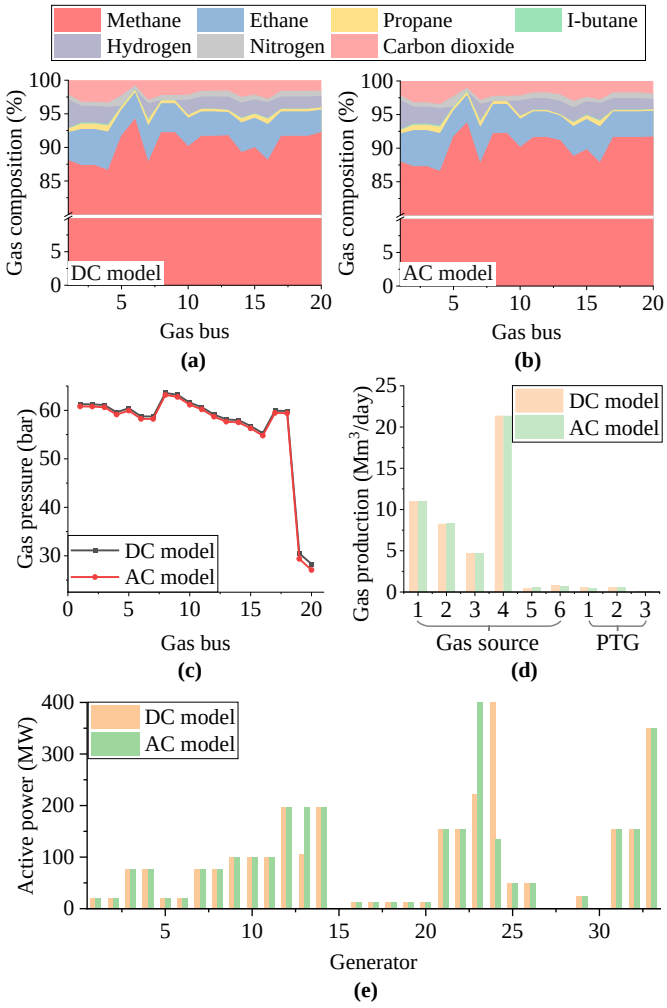

Fig. 9. Comparison of IEGS conditions with DC and AC electric power flow models

cost of adjustive gas is only 1.5 times of the cost of natural gas, the use of adjustive gas is cost-efficient. Comparing Cases 6 and 7, we find that with more relaxed security requirements, less adjustive gas is required to achieve a higher level of alternative gas injection. The operating cost is also reduced by 4.80%. Comparing Case 6 and Case 8, we find that the increase in the unit cost of adjustive gas can affect the IEGS conditions. Compared with Case 6, the gas production of PTG and the injection of adjustive gases are reduced by 8.98% and 63.45%, respectively. However, the total cost increases slightly by 0.51%. This indicates that when the unit cost of adjustive gas becomes more than three times of the unit cost of natural gas, the use of adjustive gas may become less cost-efficient.

3) Impact of PTG subsidy: To demonstrate the impacts of subsidy on the PTG's hydrogen production, we compare four

TABLE V
IMPACT ANALYSIS OF PTG SUBSIDY

	Case 9	Case 10	Case 11	Case 12
Type of Generator #23	Renewable generator	Renewable generator	GPP	Renewable generator
Subsidy for green gas production ($/m^3)	0.15	0	0	0
Capacity of transmission line #28, 31, 32, and 33	Original values	Original values	Original values	3 times of original values
Gas production of PTG #1 (Mm^3/day)	0.5551	0.5497	0	0
Gas production of PTG #2 (Mm^3/day)	1.5126	1.5123	0	0
Gas production of PTG #3 (Mm^3/day)	0.2685	0.2659	0	0

cases. In all four cases, the PTG capacity is set to 2 Mm^3/day. Other parameters are listed in the top half of Table. V.

The gas productions of PTGs in four cases are presented in the bottom half of Table. V. Comparing Cases 9 and 10, we can find that canceling subsidies has a limited impact on the gas production of PTGs. The total gas production of PTGs in Case 10 is only 0.36% lower than in Case 9. This is because the marginal generating cost for renewable generators is near zero. Using electricity at near-zero cost to produce gas to satisfy the gas demand is beneficial from the system's view. However, in Cases 11 and 12 where the generating cost and transmission capacity increase, the gas productions of PTGs directly decrease to zero. This is because using electricity from fossil-fired units to produce hydrogen is not cost-effective in most scenarios. If there are surplus renewable generations but no network congestion, the renewable generation will be used to cover the electricity baseload first rather than to produce hydrogen.

4) Impact of wind uncertainty: To investigate the impacts of wind uncertainties, three cases, Case 13, 14, and 15, are set. Considering the high fluctuation and intermittence of the wind powers, they are set to 50%, 100%, and 200% of the original value in three cases, respectively. The hydrogen production capacities of PTGs are all set to 3 Mm^3/day. To fully demonstrate the impacts on the security indices, the results with/without the security constraints are also compared. The four security indices and gas productions of PTGs are presented in Fig. 10.

From Fig. 10.(a)-(d), we find that with the increase in renewable generation, the security indices become more fluctuated. For example, the average deviation of nodal GCVs to the baseline in Case 15 is 31.35% higher than in Case 13. Nonetheless, the proposed OEF model still effectively contains the security indices within an acceptable range. For example, in Fig. 10.(b), the hydrogen injection significantly increases the Weaver flame speed factors. If we do not constrain the security, the Weaver flame speed factors at gas bus #4, 10, 14, 15, and 16 in Case 15 will exceed the upper limit (+10%), as shown in the purple dash line. However, with the proposed OEF model, the Weaver flame speed factor is successfully contained.

The wind power level also affects the operating mode of PTGs. As in Fig. 10. (e), from Case 13 to 14 and to 15, with the increase of wind power level, the gas productions of PTGs gradually increase. The total gas productions of PTGs with security constraints in Case 15 are 509.66% and 68.72% higher than in Cases 13 and 14, respectively. This is because the renewable generator has a lower marginal cost, which is cost-beneficial to be used to produce green gas. In the

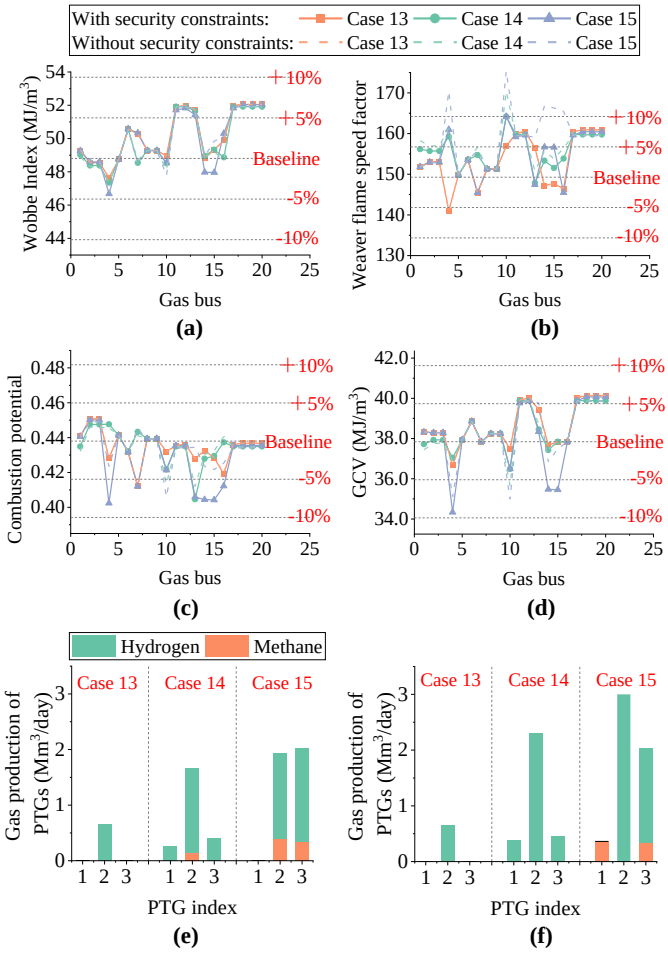

Fig. 10. Operating condition of IEGS with different wind power levels: (a) Wobbe index; (b) Weaver flame speed factor; (c) Combustion potential; (d) GCV; (e) gas productions of PTGs with security constraints; (f) gas productions of PTGs without security constraint.

meantime, we also notice that the marginal increments of gas production in Case 15 and Case 14 in Fig. 10. (e) is decreasing compared with Fig. 10. (f). It means that if we continue to increase renewable generation, the gas production of PTG may probably no longer increase due to security constraints. Instead, PTGs tend to produce more methane.

5) Impact of load fluctuation: To investigate the impacts of load fluctuations, three cases, Cases 16, 17, and 18, are added. The load levels in three cases are set to 80%, 100%, and 105%, respectively. The hydrogen production capacities of PTGs are set to 3 Mm^3/day. The four security indices and gas productions of PTGs are presented in Fig. 11.

From Fig. 11.(a) and Fig. 11.(b), we find that with the increase in load level, the gas productions from PTGs increase slightly. From Cases 16 to 17 and to 18, the gas productions of

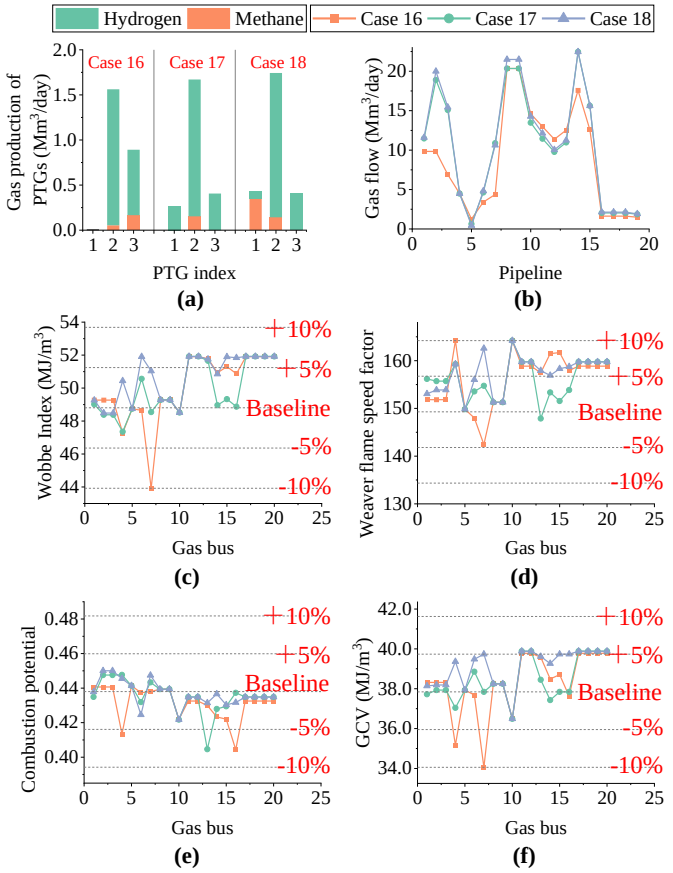

Fig. 11. Operating condition of IEGS with different load levels: (a) gas productions of PTGs; (b) gas flow; (c) Wobbe index; (d) Weaver flame speed factor; (e) Combustion potential; (f) GCV.

PTGs are increased by 4.73% and 5.29%, respectively. From Cases 16 to 17, not all increased gas loads are satisfied by the PTGs. Instead, most of them are satisfied by the natural gas source. The gas flows from the gas sources (e.g., the gas flow in pipelines #1-3, 7, and 14) increase dramatically. While from Case 17 to 18, the gas flow pattern does not change much. Most of the increased gas load is supplied by PTGs, which indicates the PTG can also serve for peak regulation in the gas system. From 11.(c) to Fig. 11.(f), we can see that although the Wobbe index at gas bus #7, Weaver flame speed factors at gas bus #4 and 11, and GCV at gas bus #7 in some cases is at +10% or -10%, all the security of IEGS is strictly restricted within the given boundaries with load fluctuations.

6) Impact of IEGS topology: To investigate the impacts of different topologies of the electricity and gas systems on the performance of the proposed OEF model, three cases are set. Case 19 is the base case where the IEGS is intact. In Case 20, electric branch #30 (between electricity buses #17 and 18) fails due to the outage. In Case 21, pipeline #7 (between gas bus #4 and 14) fails due to rupture failure. It is worth mentioning that due to component failure, the IEGS may not always be balanced. Thus, we introduce electricity and gas load curtailments as extra variables into the OEF model. The temporary relaxation of security requirements is allowed [46].

From Fig. 12, we find that the change of topology can affect the operating condition of IEGS. From Case 19 to 20, with the failure of the electricity branch, the gas production of PTGs

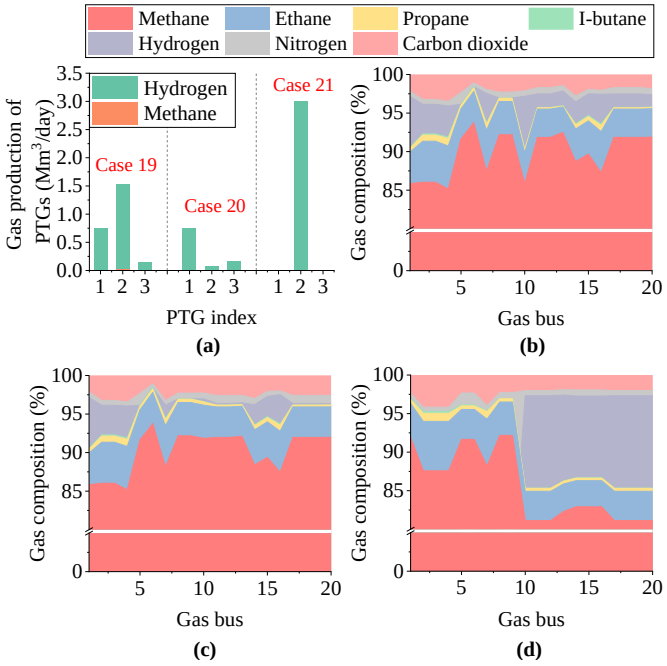

Fig. 12. Operating condition of IEGS with different topologies of the electricity and gas systems: (a) gas productions of PTGs; (b) gas composition in Case 19; (c) gas composition in Case 20; (d) gas composition in Case 21.

reduces by 59.08%, especially for PTG #2. PTG #2 is located on the electricity bus #17. The renewable generator is located at electricity bus #18, which is connected to #17 through the electric branch #30. Thus, the failure of electric branch #30 could reduce the renewable generation transported from #18 to #17, which leads to a decrease in the gas production of PTG #2. Correspondingly, the molar fractions of hydrogen in Case 20 at gas bus#10 - 13 and 17-20 are also lower than in Case 19.

From Case 19 to 21, due to the failure of pipeline #7, the gas system is isolated into two parts, namely, the north part and the south part. The PTG #1 and 3 are located in the north part, where the gas supply is relatively sufficient. Therefore, the gas productions of these two PTGs are near zero. On the contrary, the gas supply of the south part is not sufficient enough. Therefore, PTG #2 operates at the maximum capacity, and the molar fractions of hydrogen from gas bus #10 to 20 are higher than in Case 19.

7) Impacts of key components: To investigate the impacts of key components, four cases are constructed. In Case 22, the locations of PTGs are changed to gas buses #16, 20, and 19, respectively. In Case 23, the locations of renewable generation are changed to #1. In Case 24, the locations of GPPs are changed to gas bus #15, 16, 19, and 20, respectively.

Comparing Case 22 and Case 19, we find that the locations of PTGs are important for promoting alternative gas injections. In Case 22, the PTGs are at the end of the gas pipeline routes. The injected hydrogen or methane cannot be fully mixed with other gases to balance the security indices. Therefore, the gas injections from PTGs are near zero, as shown in Fig. 13. (a). Correspondingly, as shown in Fig. 13. (b), the molar fraction of hydrogen in Case 22 is near zero.

In Case 23, the gas productions of PTGs are also reduced

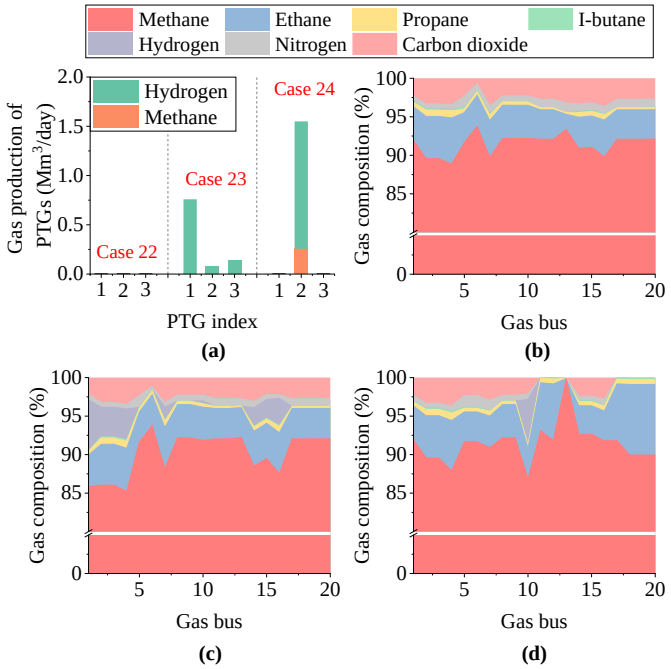

Fig. 13. Operating condition of IEGS with different locations of key components: (a) gas productions of PTGs; (b) gas composition in Case 22; (c) gas composition in Case 23; (d) gas composition in Case 24.

due to the distant location of renewable generations. Case 23 is similar to Case 20 which has electric branch failure, the improper location of renewable generation also leads to less electricity consumption of PTGs. The gas production of PTG #1 is still considerable because it is at electricity bus #10, which is near to electricity bus #1. The gas composition in Case 23 also presents a similar pattern as in Case 20.

In Case 24, the gas productions of PTGs are also affected due to the improper locations of GPPs. The new locations for GPPs are at the end of pipeline routes in the south part, which increase the transportation burden for the gas system. The PTG #1 and #3 are at the north part of the gas system. The upper bounds of the nodal gas pressure limit the ability for the gas in the north part to be transported to the end of pipeline routes in the south part. Thus, the gas productions of PTG #1 and 3 are near zero. On the contrary, the PTG #2 at gas bus #10 increases. Correspondingly, except for the gas buses near #10, the molar fractions of hydrogen in the rest of the gas buses are also near zero.

D. *Validation Using a Large-scale Case*

To further validate the effectiveness of the proposed OEF model and solution method, A larger test case, the natural gas transmission system in the UK, is used in this Section, as presented in Fig. 14. It has 160 buses, 237 pipelines, 11 gas sources, and 21 compressor stations. The network structure data are acquired from the National Grid [47]. The operation data, including the gas supply and demand on Oct 30th, 2022, is used [48]. The hydrogen injections are located at St. Fergus and Isle of Grain, respectively, according to the HyNTS project [49]. The hydrogen production capabilities are assumed to be 5 Mm^3/day.

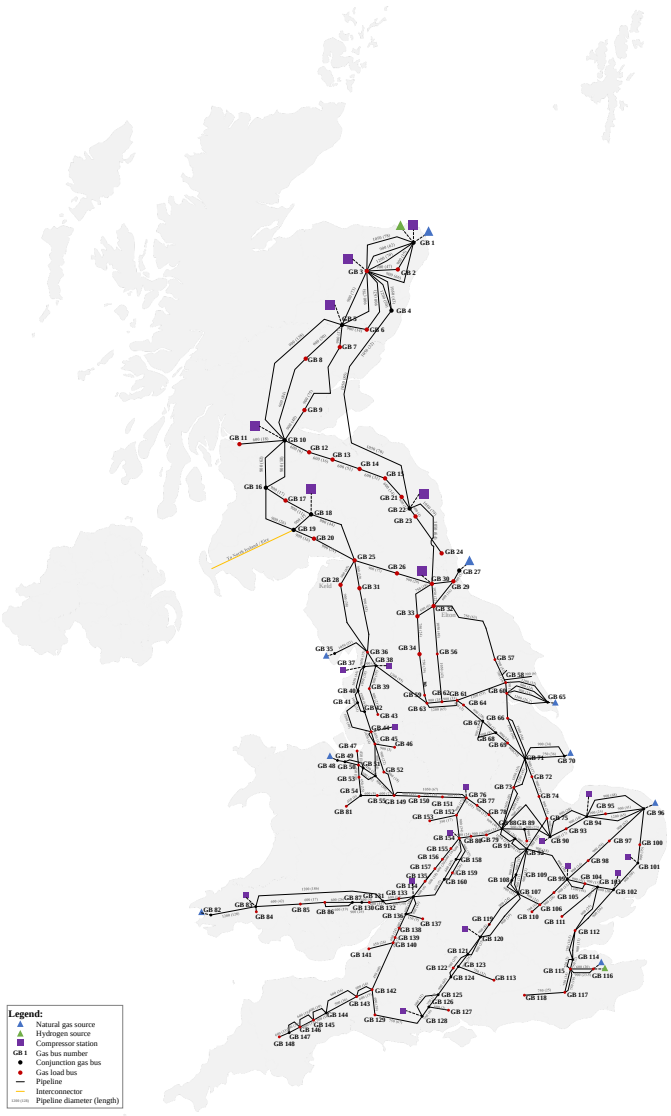

Fig. 14. Schematic diagram of the gas transmission system in the UK.

The computation time using the proposed solution method is 57.86 s. The operating condition of the UK's gas system is presented in Fig. 15. We can find that the security indices are all contained within the specified ranges. The peak molar fraction of hydrogen 9.84% appears at gas bus #116. This is because the 5 Mm^3/day hydrogen is also injected at gas bus #116, which increases the molar fraction of hydrogen in this bus and adjacent buses. Correspondingly, the Weaver flame speed factor also reaches the peak value at gas bus #116.

VII. Conclusions

This paper proposes an OEF model for IEGS with alternative gas injections, and develops solution methods that ensure the proposed model can be handled more robustly by commercial solvers. Six security indices and detailed physical characteristics for gas mixtures are considered to ensure the secure operation of the IEGS. Different forms of nonlinear terms are flexibly addressed by various convex optimization techniques. Advanced sequential programming procedures are utilized to improve computation efficiency.

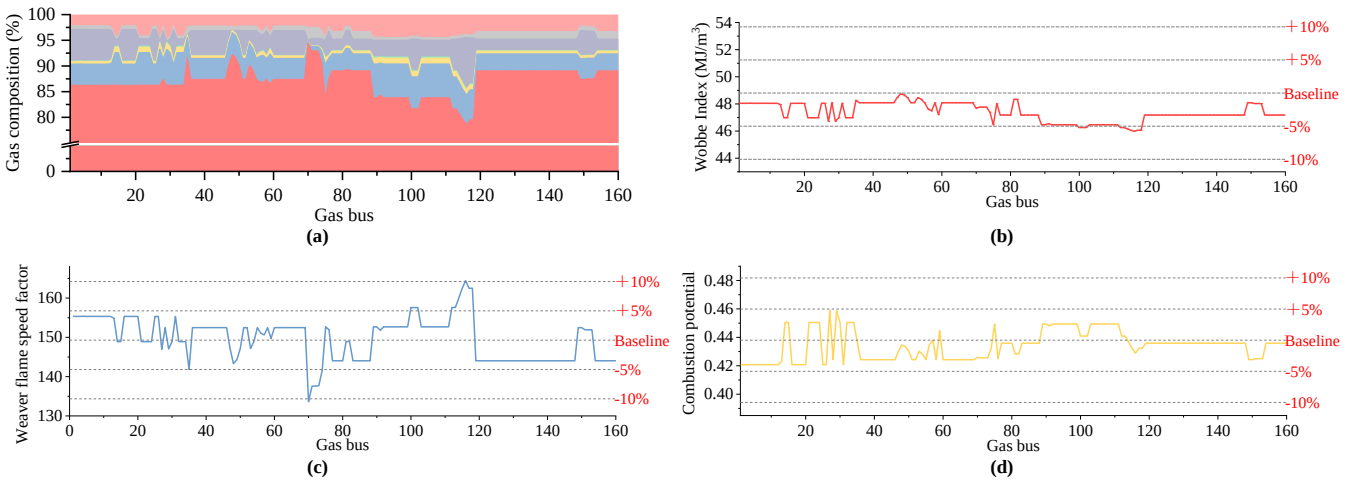

Fig. 15. Operating conditions of the Britain gas system: (a) gas composition; (b) Wobbe index; (c) Weaver flame speed factor; (d) combustion potential.

In the case studies, we validate the computation efficiency of the proposed solution methods is 96.44% superior to traditional mixed-integer nonlinear solvers. From the numerical results, we also validate that the injection of alternative gas can cause up to 4.32% variations in the nodal gas pressure. Nonetheless, the proposed OEF model can still effectively contain the security indices of IEGS within the acceptable range. By further using adjustive gas, the operating cost can be reduced by 4.35 %. Through the comparison of different cases, we demonstrate the application of the proposed OEF model. We find that various factors and uncertainties, including the tolerances of security indices, the capacities and locations of PTGs and renewable generators, IEGS topologies, load levels, wind uncertainties, etc., can have significant impacts on alternative gas injections and IEGS operation. For example, with the increase of renewable generation, the Weaver flame speed factor will increase, while the Wobbe index and GCV will decrease. If the locations of renewable generations are distant from PTGs or are at the ends of pipeline routes, the gas production of PTG will decrease. If the GPPs are at the ends of pipeline routes, the alternative gas injection may also decrease.

Besides the secured and optimal operation of IEGS, the proposed OEF also provides a fundamental tool for further analysis of IEGS with alternative gas, such as economic dispatch, optimal load shedding, reliability evaluation, unit commitment, long-term planning, etc. With the decarbonization of energy systems, hydrogen injection may become a more appealing option in the next few decades. The application of the proposed OEF model will also be more promising in the future.

APPENDIX

A. Calculation of Compressibility Factor for Gas Mixture

When the gas composition in the pipeline changes constantly and dramatically, it will be inaccurate to regard the gas mixture as the ideal gas. Therefore, the compressibility of the gas cannot be regarded as a constant, which should be modified by [20], [35]:

$$Z_{i,j}^3 - Z_{i,j}^2 + Z_{i,j}(A_{i,j} - B_{i,j} - B_{i,j}^2) - A_{i,j}B_{i,j} = 0 \quad (60)$$

$$A_{i,j} = 0.42747 \frac{p_{i,j}^{\text{av}}}{(T^{\text{gas}})^2} \left(\sum_{r \in \mathcal{R}} \frac{x_{i,j,r} T_r^{\text{C}}}{\sqrt{p_r^{\text{C}}}} \right)^2 \quad (61)$$

$$B_{i,j} = 0.08664 \frac{p_{i,j}^{\text{av}}}{T^{\text{gas}}} \sum_{r \in \mathcal{R}} \frac{x_{i,j,r} T_r^{\text{C}}}{p_r^{\text{C}}} \quad (62)$$

$$p_{i,j}^{\text{av}} = \frac{2}{3} \left(p_i + p_j - \frac{p_i p_j}{p_i + p_j} \right) \quad (63)$$

where $A_{i,j}$ and $B_{i,j}$ are the parameters for compresibility calculation in pipeline ij; $p_{i,j}^{\text{av}}$ is the average pressure in pipeline ij; T_r^{C} and p_r^{C} are the critical temperature and pressure of gas component r, respectively.

B. Proof of Convergence of Sequential Programming

The OEF problem can be written in a compact form as:

$$\min_{x,y,\boldsymbol{\sigma}} \boldsymbol{f}'(\boldsymbol{x}) = \boldsymbol{c}\boldsymbol{x} + \alpha^{(v)} \mathbf{1}^T \boldsymbol{\sigma} \quad (64)$$

s.t.

$$\boldsymbol{a}\boldsymbol{x} + \boldsymbol{b}\boldsymbol{y} + \boldsymbol{e}\boldsymbol{\sigma} \leq \boldsymbol{d} \quad (65)$$

$$\boldsymbol{h}(\boldsymbol{x}) \leq 0 \quad (66)$$

$$\hat{\boldsymbol{h}}(\boldsymbol{x}, \boldsymbol{x}^{(v)}) + \boldsymbol{\sigma} \geq 0 \quad (67)$$

$$\boldsymbol{y} \in \{0, 1\} \quad (68)$$

where $\boldsymbol{a}$, $\boldsymbol{b}$, $\boldsymbol{c}$, and $\boldsymbol{d}$ are coefficient matrices, respectively; $\boldsymbol{x}$ and $\boldsymbol{y}$ are continuous and binary optimization variables, respectively; $\boldsymbol{h}(\boldsymbol{x})$ is the SOC function; $\alpha^{(v)}$ is the penalty factor in v_{th} iteration in sequential programming; $\boldsymbol{\sigma}$ is the slack variable; $\boldsymbol{x}^{(v)}$ is the value of $\boldsymbol{x}$ in v_{th} iteration in sequential programming. $\hat{\boldsymbol{h}}(\boldsymbol{x}, \boldsymbol{x}^{(v)})$ is the Taylor expansion of $\boldsymbol{h}(\boldsymbol{x})$ around point $\boldsymbol{x}^{(v)}$, which can be written as:

$$\hat{\boldsymbol{h}}(\boldsymbol{x}, \boldsymbol{x}^{(v)}) = \boldsymbol{h}(\boldsymbol{x}^{(v)}) + \nabla \boldsymbol{h}(\boldsymbol{x}^{(v)})^T (\boldsymbol{x} - \boldsymbol{x}^{(v)}) \quad (69)$$

Since $\boldsymbol{h}(\boldsymbol{x})$ is convex, we can know that:

$$\hat{\boldsymbol{h}}(\boldsymbol{x}, \boldsymbol{x}^{(v)}) \leq \boldsymbol{h}(\boldsymbol{x}) \quad (70)$$

We denote the optimal solution of the OEF problem in v_{th} iteration as $\boldsymbol{x}^{(v)}$ and $\boldsymbol{\sigma}^{(v)}$. Then, we have:

$$\hat{\boldsymbol{h}}(\boldsymbol{x}^{(v)}, \boldsymbol{x}^{(v-1)}) + \boldsymbol{\sigma}^{(v)} \geq 0 \quad (71)$$

Subscribe the solution of v_{th} iteration into the (67) in $(v+1)_{th}$ iteration, the left hand side can be written as $\hat{\boldsymbol{h}}(\boldsymbol{x}^{(v)}, \boldsymbol{x}^{(v)}) + \boldsymbol{\sigma}^{(\boldsymbol{v})}$. According to (70), we know that $\hat{\boldsymbol{h}}(\boldsymbol{x}^{(v)}, \boldsymbol{x}^{(v)}) + \boldsymbol{\sigma}^{(\boldsymbol{v})} \geq \hat{\boldsymbol{h}}(\boldsymbol{x}^{(v)}, \boldsymbol{x}^{(v-1)})$. Then according to (71), we can assert that:

$$\hat{\boldsymbol{h}}(\boldsymbol{x}^{(v)}, \boldsymbol{x}^{(v)}) + \boldsymbol{\sigma}^{(\boldsymbol{v})} \geq 0 \tag{72}$$

which means the the optimal solution in v_{th} iteration, $(\boldsymbol{x}^{(v)}, \boldsymbol{\sigma}^{(\boldsymbol{v})})$, is a feasible solution in $(v+1)_{th}$ iteration. Therefore, we can know that:

$$\boldsymbol{f}'(\boldsymbol{x}^{(v+1)}, \boldsymbol{\sigma}^{(\boldsymbol{v+1})}) \leq \boldsymbol{f}'(\boldsymbol{x}^{(v)}, \boldsymbol{\sigma}^{(\boldsymbol{v})}) \tag{73}$$

where $(\boldsymbol{x}^{(v+1)}, \boldsymbol{\sigma}^{(v+1)})$ is the optimal solution in $(v+1)_{th}$ iteration. It means that as the iteration proceeds, the objective function will decrease, or at least will be no greater than the value in the last iteration. Because the original problem is feasible and has a finite objective function value, there must exist a convergence threshold ϵ that satisfies:

$$|\boldsymbol{f}'(\boldsymbol{x}^{(v+1)}, \boldsymbol{\sigma}^{(\boldsymbol{v+1})}) - \boldsymbol{f}'(\boldsymbol{x}^{(v)}, \boldsymbol{\sigma}^{(\boldsymbol{v})})| < \epsilon \tag{74}$$

Therefore, we can claim that the proposed sequential cone programming can converge.

There is another potential issue that due to the binary variable in (65), the OEF problem is non-convex and the solution of the binary variable (which represents the gas flow direction) may change during the iterations. Practically speaking, because the system states do not change dramatically, it can be expected that the direction of gas flow can be stabilized quickly after a few iterations. On this basis, the problem can be regarded as convex after a few iterations, and the above statement still holds [50].

Though the sequential cone programming can converge, whether the optimal solution of the reformulated problem will converge to the optimal solution of the original problem depends on whether the slack variable $\boldsymbol{\sigma}$ can converge to zero. To ensure slack variables $\boldsymbol{\sigma}$ converge to zero, the value of the maximum penalty factor α^{max} should be greater than the exact penalty parameter α^{max*}. According to [38], the exact penalty factor should be greater than the largest optimal dual variable. However, the exact penalty parameter is difficult to be determined in practice. Therefore, the initial penalty factor α at the beginning of sequential programming should be small to find the feasible solution quickly. As the iteration proceeds, the upper limit for penalty factor α^{max} should be large, but not so large that causes numerical problems [51], [52]. Under these conditions, the proposed sequential cone programming can converge to the optimum more quickly.

REFERENCES

[1] Z. Zhang, C. Wang, H. Lv, F. Liu, H. Sheng, and M. Yang, "Day-ahead optimal dispatch for integrated energy system considering power-to-gas and dynamic pipeline networks," *IEEE Transactions on Industry Applications*, vol. 57, no. 4, pp. 3317–3328, Apr. 2021.

[2] Safe operation for one year with 10% hydrogen blending, new breakthrough on first natural gas with hydrogen blending demonstration in China . [Online]. Available: https://new.qq.com/rain/a/20211019A04KVF00.

[3] HyDeploy Project – Project Close Down Report. [Online]. Available: https://hydeploy.co.uk/app/uploads/2022/06/HyDeploy-Close-Down-Report_Final.pdf.

[4] K. Stolecka, "Hazards of hydrogen transport in the existing natural gas pipeline network," *Journal of Power Technologies*, no. 4, pp. 329–335, Sep. 2018.

[5] T. Briggs, "The combustion and interchangeability of natural gas on domestic burners," *Combustion*, vol. 4, no. 3, 2014.

[6] K. Altfeld and D. Pinchbeck, "Admissible hydrogen concentrations in natural gas systems," *Gas Energy*, vol. 2103, no. 03, pp. 1–2, Mar. 2013.

[7] D. Haeseldonckx and W. D'haeseleer, "The use of the natural-gas pipeline infrastructure for hydrogen transport in a changing market structure," *International Journal of Hydrogen Energy*, vol. 32, no. 10-11, pp. 1381–1386, Jul-Aug. 2007.

[8] M. W. Melaina, O. Antonia, and M. Penev, "Blending hydrogen into natural gas pipeline networks: a review of key issues," *Hydrogen Knowledge Centre*, Mar. 2013.

[9] J. Schouten, J. Michels, and R. Janssen-van Rosmalen, "Effect of h2-injection on the thermodynamic and transportation properties of natural gas," *International Journal of Hydrogen Energy*, vol. 29, no. 11, pp. 1173–1180, 2004.

[10] F. Uilhoorn, "Dynamic behaviour of non-isothermal compressible natural gases mixed with hydrogen in pipelines," *International Journal of Hydrogen Energy*, vol. 34, no. 16, pp. 6722–6729, 2009, 4th Dubrovnik Conference.

[11] G. Guandalini, P. Colbertaldo, and S. Campanari, "Dynamic quality tracking of natural gas and hydrogen mixture in a portion of natural gas grid," *Energy Procedia*, vol. 75, pp. 1037–1043, 2015, clean, Efficient and Affordable Energy for a Sustainable Future: The 7th International Conference on Applied Energy (ICAE2015).

[12] M. Abeysekera, J. Wu, N. Jenkins, and M. Rees, "Steady state analysis of gas networks with distributed injection of alternative gas," *Applied Energy*, vol. 164, pp. 991–1002, Feb. 2016.

[13] G. Guandalini, P. Colbertaldo, and S. Campanari, "Dynamic modeling of natural gas quality within transport pipelines in presence of hydrogen injections," *Applied Energy*, vol. 185, pp. 1712–1723, Jan. 2017.

[14] Z. Zhang, I. Saedi, S. Mhanna, K. Wu, and P. Mancarella, "Modelling of gas network transient flows with multiple hydrogen injections and gas composition tracking," *International Journal of Hydrogen Energy*, vol. 47, no. 4, pp. 2220–2233, 2022.

[15] D. Zhou, C. Wang, S. Yan, Y. Yan, Y. Guo, T. Shao, T. Li, X. Jia, and J. Hao, "Dynamic modeling and characteristic analysis of natural gas network with hydrogen injections," *International Journal of Hydrogen Energy*, vol. 47, no. 78, pp. 33 209–33 223, 2022.

[16] M. Cavana, A. Mazza, G. Chicco, and P. Leone, "Electrical and gas networks coupling through hydrogen blending under increasing distributed photovoltaic generation," *Applied Energy*, vol. 290, p. 116764, 2021.

[17] L. Cheli, G. Guzzo, D. Adolfo, and C. Carcasci, "Steady-state analysis of a natural gas distribution network with hydrogen injection to absorb excess renewable electricity," *International Journal of Hydrogen Energy*, vol. 46, no. 50, pp. 25 562–25 577, 2021.

[18] S. Zhang, S. Wang, Z. Zhang, J. Lyu, H. Cheng, M. Huang, and Q. Zhang, "Probabilistic multi-energy flow calculation of electricity-gas integrated energy system with hydrogen injection," *IEEE Transactions on Industry Applications*, vol. 58, no. 2, pp. 2740–2750, Jul. 2021.

[19] D. Zhou, S. Yan, D. Huang, T. Shao, W. Xiao, J. Hao, C. Wang, and T. Yu, "Modeling and simulation of the hydrogen blended gas-electricity integrated energy system and influence analysis of hydrogen blending modes," *Energy*, vol. 239, p. 121629, 2022.

[20] I. Saedi, S. Mhanna, and P. Mancarella, "Integrated electricity and gas system modelling with hydrogen injections and gas composition tracking," *Applied Energy*, vol. 303, p. 117598, Dec. 2021.

[21] A. De Corato, I. Saedi, S. Riaz, and P. Mancarella, "Aggregated flexibility from multiple power-to-gas units in integrated electricity-gas-hydrogen distribution systems," *Electric Power Systems Research*, vol. 212, p. 108409, 2022.

[22] P. Zhao, C. Gu, Z. Hu, D. Xie, I. Hernando-Gil, and Y. Shen, "Distributionally robust hydrogen optimization with ensured security and multi-energy couplings," *IEEE Transactions on Power Systems*, vol. 36, no. 1, pp. 504–513, Jun. 2020.

[23] P. Zhao, X. Lu, Z. Cao, C. Gu, Q. Ai, H. Liu, Y. Bian, and S. Li, "Volt-var-pressure optimization of integrated energy systems with hydrogen injection," *IEEE Transactions on Power Systems*, vol. 36, no. 3, pp. 2403–2415, 2021.

[24] S. Mhanna, I. Saedi, P. Mancarella, and Z. Zhang, "Coordinated operation of electricity and gas-hydrogen systems with transient gas flow and

hydrogen concentration tracking," *Electric Power Systems Research*, vol. 211, p. 108499, 2022.
[25] Gas Exchangeability in Western Australia – Gas quality specifications of interconnected pipeline systems. [Online]. Available: https://www.erawa.com.au/cproot/6284/2/20071220%20Gas%20Exchangeability%20in%20Western%20Australia%20-%20Gas%20Quality%20Specifications%20of%20Interconnected%20Pipeline%20Systems.pdf.
[26] J. Klimstra, "Interchangeability of gaseous fuels—the importance of the wobbe-index," *SAE Transactions*, pp. 962–972, 1986.
[27] Injecting hydrogen into the gas network – a literature search. [Online]. Available: https://www.h2knowledgecentre.com/content/policypaper1193.
[28] M. Bus, "Review of the impact of hydrogen addition to natural gas on gas turbine combustion," Jun. 2013.
[29] E. R. Weaver, "Formulas and graphs for representing the interchangeability of fuel gases," *Journal of Research of the National Bureau of Standards*, vol. 46, no. 3, pp. 214–245, 1951.
[30] D. Quintero-Coronel, Y. Lenis-Rodas, L. Corredor, P. Perreault, A. Bula, and A. Gonzalez-Quiroga, "Co-gasification of biomass and coal in a top-lit updraft fixed bed gasifier: Syngas composition and its interchangeability with natural gas for combustion applications," *Fuel*, vol. 316, p. 123394, 2022.
[31] T. A. Williams, "Technical background and issues of gas interchangeability," *AGA Staff Paper*, Apr. 2006.
[32] C. Halpern, "Measurement of flame speeds by a nozzle burner method," *Journal of Research of the National Bureau of Standards*, vol. 60, no. 6, pp. 535–546, 1958.
[33] A. Osiadacz, "Simulation and analysis of gas networks," 1987.
[34] I. Eames, M. Austin, and A. Wojcik, "Injection of gaseous hydrogen into a natural gas pipeline," *International Journal of Hydrogen Energy*, vol. 47, no. 61, pp. 25 745–25 754, Apr. 2022.
[35] G. Soave, "Equilibrium constants from a modified redlich-kwong equation of state," *Chemical Engineering Science*, vol. 27, no. 6, pp. 1197–1203, Jun. 1972.
[36] L. Gan and S. H. Low, "Optimal power flow in direct current networks," *IEEE Transactions on Power Systems*, vol. 29, no. 6, pp. 2892–2904, 2014.
[37] Y. Wen, X. Qu, W. Li, X. Liu, and X. Ye, "Synergistic operation of electricity and natural gas networks via admm," *IEEE Transactions on Smart Grid*, vol. 9, no. 5, pp. 4555–4565, Feb. 2017.
[38] T. Lipp and S. Boyd, "Variations and extension of the convex–concave procedure," *Optimization and Engineering*, vol. 17, no. 2, pp. 263–287, Nov. 2016.
[39] C. Feng, B. Liang, Z. Li, W. Liu, and F. Wen, "Peer-to-peer energy trading under network constraints based on generalized fast dual ascent," *IEEE Transactions on Smart Grid*, pp. 1–1, Mar. 2022.
[40] H. Zhou, Z. Li, J. Zheng, Q. Wu, and H. Zhang, "Robust scheduling of integrated electricity and heating system hedging heating network uncertainties," *IEEE Transactions on Smart Grid*, vol. 11, no. 2, pp. 1543–1555, Sep. 2019.
[41] S. Wang, Y. Ding, C. Ye, C. Wan, and Y. Mo, "Reliability evaluation of integrated electricity–gas system utilizing network equivalent and integrated optimal power flow techniques," *Journal of Modern Power Systems and Clean Energy*, vol. 7, no. 6, pp. 1523–1535, Nov. 2019.
[42] C. Grigg, P. Wong, P. Albrecht, R. Allan, M. Bhavaraju, R. Billinton, Q. Chen, C. Fong, S. Haddad, S. Kuruganty *et al.*, "The IEEE reliability test system-1996. A report prepared by the reliability test system task force of the application of probability methods subcommittee," *IEEE Transactions on Power Systems*, vol. 14, no. 3, pp. 1010–1020, Aug. 1999.
[43] D. De Wolf and Y. Smeers, "The gas transmission problem solved by an extension of the simplex algorithm," *Management Science*, vol. 46, no. 11, pp. 1454–1465, Nov. 2000.
[44] H. Hui, P. Siano, Y. Ding, P. Yu, Y. Song, H. Zhang, and N. Dai, "A transactive energy framework for inverter-based hvac loads in a real-time local electricity market considering distributed energy resources," *IEEE Transactions on Industrial Informatics*, vol. 18, no. 12, pp. 8409–8421, Feb. 2022.
[45] H. Hui, Y. Chen, S. Yang, H. Zhang, and T. Jiang, "Coordination control of distributed generators and load resources for frequency restoration in isolated urban microgrids," *Applied Energy*, vol. 327, p. 120116, Dec. 2022.
[46] Gas Safety (Management) Regulations. [Online]. Available: https://www.legislation.gov.uk/uksi/1996/551/introduction/made.
[47] Gas Ten Year Statement (GTYS). [Online]. Available: https://www.nationalgrid.com/gas-transmission/insight-and-innovation/gas-ten-year-statement-gtys.
[48] Transmission operational data. [Online]. Available: https://www.nationalgrid.com/gas-transmission/data-and-operations/transmission-operational-data.
[49] HyNTS FutureGrid Phase 1 – National Grid Gas Transmission. [Online]. Available: https://www.ofgem.gov.uk/publications/hynts-futuregrid-phase-1-national-grid-gas-transmission.
[50] Y. He, M. Yan, M. Shahidehpour, Z. Li, C. Guo, L. Wu, and Y. Ding, "Decentralized optimization of multi-area electricity-natural gas flows based on cone reformulation," *IEEE Transactions on Power Systems*, vol. 33, no. 4, pp. 4531–4542, Dec. 2018.
[51] Z. Tian and W. Wu, "Recover feasible solutions for socp relaxation of optimal power flow problems in mesh networks," *IET Generation, Transmission & Distribution*, vol. 13, no. 7, pp. 1078–1087, Mar.
[52] W. Wei, J. Wang, N. Li, and S. Mei, "Optimal power flow of radial networks and its variations: A sequential convex optimization approach," *IEEE Transactions on Smart Grid*, vol. 8, no. 6, pp. 2974–2987, Mar. 2017.